6-2022

Evaluation of an Equivalent Mean Grain Size Diameter to Rationally Predict the Erodibility of Fine Riverbed Soils in Nebraska

Basil Abualshar
University of Nebraska-Lincoln, babualshar2@huskers.unl.edu

Evaluation of an Equivalent Mean Grain Size Diameter to Rationally Predict the Erodibility of Fine Riverbed Soils in Nebraska

by

Basil Abualshar

A THESIS

Presented to the Faculty of

The Graduate College at the University of Nebraska

In Partial Fulfillment of Requirements

For the Degree of Master of Science

Major: Civil Engineering

Under the Supervision of Professor Chung R. Song

Lincoln, Nebraska

June, 2022

Evaluation of an Equivalent Mean Grain Size Diameter to Rationally Predict the Erodibility of Fine Riverbed Soils in Nebraska

Basil Abualshar, M.S

University of Nebraska, 2022

Advisor: Chung R. Song

The erosion of riverbed soils under the bridges is one of the major reasons that cause bridge closure or failure leading to a significant effect on the local economy. One of the commonly used methods to predict the erosion rate of soils is the excess shear stress method, which is based on two parameters describing the erodibility behavior; the erodibility coefficient and the critical shear stress. On the other hand, studies showed that the mean grain size diameter D_{50} could be correlated to the erosion resistance of soils on the riverbed, usually for cohesionless soils but not applicable for cohesive soils currently. It is because the cohesive soils are small and typically plate or needle shape, and erosion may be affected by several intergranular forces which are not prominent in cohesionless soils. Therefore, if D_{50} technique revised to be used for cohesive soils, the prediction of riverbed erosion may become much convenient.

This study aimed to find the equivalent sand particle diameter (D_{50}) experimentally for fine-grained soils in Nebraska around Lincoln so that the erosion of these fine-grained soils can be predicted conveniently. To achieve this goal, 17 soil samples from four different rivers around Lincoln in Nebraska were tested using the Mini Jet Erosion

Testing device to obtain the erodibility coefficient and the critical shear stress. Then, the results were analyzed to conveniently obtain the equivalent grain size of the sand for the same critical shear stress graphically. With this procedure, engineers may conveniently analyze the erosion of riverbed fine-grained soils based on popular software which utilize D_{50}.

Acknowledgements

I would like to express my gratitude and deep appreciation to my advisor Dr. Chung R. Song, for his continuous support and being such a great mentor. He stood by my side and guided me at all times. Furthermore, he was always optimistic and helped me to be positive despite all the difficulties during the research.

I would like to thank my thesis committee members, Dr. Jongwan Eun, Dr. Junke Guo, and Dr. Richard L. Wood, for serving my thesis committee.

I would like to thank Dr. Binyam Bekele for his assistance, friendship, and advice during my laboratory work.

Last but not least, I would like to thank the Nebraska Department of Transportation (NDOT) for the financial support.

Table of Contents

Chapter 1 1
Introduction 1
1.1 Background 1
1.2 Research Objectives 2
Chapter 2 3
Literature review 3
2.1 Erosion Mechanism 3
2.2 Testing Methods 5
2.2.1 Jet Erosion Test (JET) 6
2.2.2 Mini Jet Erosion Test (Mini-JET) 8
2.2.3 Erosion Function Apparatus (EFA) 9
2.2.4 Rotating Cylinder Test (RCT) 11
2.2.5 The University of Mississippi Erosion Testing Bed (UMETB) 12
2.3 Development of the Excess Shear Stress Parameters for Circular Jets. 14
2.3.1 Hanson & Cook (1997) Derivation 14
2.3.2 The main differences between Hanson & Cook (1997) and Stein et al. (1993) derivations. 18
2.4 Prediction of the Equilibrium Erosion Depth 19
2.4.1 Blaisdell et al., (1981) Hyperbolic Technique 19
2.4.2 Duncan and Chang (1970) Hyperbolic Function 20
2.5 Factors Affecting Erosion Behavior of Cohesionless and Cohesive Soils 21
2.6 Existing correlations 22
2.6.1 For course-grained soils 22
2.6.2 For Fine-grained soils 22
Chapter 3 23
Sampling, Soil properties, Applied Testing Methods 23
3.1 Locations 23
3.2 Sampling Procedure and Samples Preparation 24
3.3 Soil Properties 25
3.4 Testing Method and Analysis Procedure 27
Chapter 4 28
Test Results and Discussion 28

4.1 Erosion Plots 28
4.2 Critical Shear Stress and Erodibility Coefficient 31
4.2.1 Magnitude of Excess Shear Stress Parameters 31
4.2.2 Sample Calculation for Beatrice S2 Sample 34
4.3 Comparison with Previous Research 40
4.3.1 Comparison with Hanson & Simon (2001) 40
4.3.2 Comparison with Simon et al. (2010) 41
4.3.3 Comparison with Briaud et al. (2017) 42
4.4 Correlation Between D_{50} and the Erodibility Coefficient 45
Chapter 5 47
Conclusions, Recommendations, and Future Studies 47
5.1 Conclusions 47
5.2 Future Studies 48
References 50
Appendix A 53
Gradation Curves 53
Appendix B 56
Mini-JET Data with Back Calculation 56

List of Figures

Figure (1): Schematic of JET by Hanson & Cook (2004) 6
Figure (2): Mini JET Device by Al-Madhhachi et al. (2013) 8
Figure (3): Schematic of EFA by Briaud et al. (1999) 10
Figure (4): a) View of outside UMETB, b) View of inside UMETB (Song et al. 2011). 12
Figure (5): Approximate Test Locations 24
Figure (6): Soil Samples Before the Erosion Test 24
Figure (7): Erosion vs. Time for Lincoln Site (Note: Sample's names are matched to these in Table (5).) 28
Figure (8): Erosion vs. Time for Wilber Site (Note: Sample's names are matched to these in Table (5).) 28
Figure (9): Erosion vs. Time for Hooper Site (Note: Sample's names are matched to these in Table (5).) 29
Figure (10): Erosion vs. Time for Beatrice Site (Note: Sample's names are matched to these in Table (5).) 29
Figure (11): Erosion vs. Time for UNL Campuses (Note: Sample's names are matched to these in Table (5).) 30
Figure (12): Erosion Charts by Briaud et al. (2017) 33
Figure (13): Duncan and Chang (1970) Hyperbolic Curve 37
Figure (14): Actual Test Data and Predicted Data Based on Duncan and Chang (1970). 37
Figure (15): Test Data vs. Back Calculated Data (Note: J_i is the initial distance from the nozzle to the soil surface) 39
Figure (16): Critical Shear Stress vs. Erodibility Coefficient Based on Hanson and Simon (2001) 40
Figure (17): Critical Shear Stress vs. Erodibility Coefficient Based on Simon et al. (2010) with Test Results in This Study 42
Figure (18): Mean Grain Size D_{50} vs. Critical Shear Stress (Replotted from Briaud et al. (2017)) 43
Figure (19): Equivalent Mean Grain Size Derivation Concept 45
Figure (20): Erodibility Coefficient vs. Mean Grain Size (Arithmetic scale) 46
Figure (21): Erodibility Coefficient vs. Mean Grain Size (log-log scale) 46
Figure (22): Gradation Curves for Lincoln Site Soils 53
Figure (23): Gradation Curves for Wilber Site Soils 53
Figure (24): Gradation Curves for Hooper Site Soils 54
Figure (25): Gradation Curves for Beatrice Site Soils 54
Figure (26): Gradation Curves for UNL City Campus Soils 55
Figure (27): Gradation Curves for UNL East Campus Soils 55
Figure (28): Depth Gauge Reading vs. Time for Lincoln Site Sample 1 (Note: J_i is the initial distance from the nozzle to the soil surface) 56
Figure (29): Depth Gauge Reading vs. Time for Lincoln Site Sample 2 (Note: J_i is the initial distance from the nozzle to the soil surface) 56

Figure (30): Depth Gauge Reading vs. Time for Lincoln Site Sample 3 (Note: J_i is the initial distance from the nozzle to the soil surface) 57
Figure (31): Depth Gauge Reading vs. Time for Lincoln Site Sample 4 (Note: J_i is the initial distance from the nozzle to the soil surface) 57
Figure (32): Depth Gauge Reading vs. Time for Wilber Site Sample 1 (Note: J_i is the initial distance from the nozzle to the soil surface) 58
Figure (33): Depth Gauge Reading vs. Time for Wilber Site Sample 2 (Note: J_i is the initial distance from the nozzle to the soil surface) 58
Figure (34): Depth Gauge Reading vs. Time for Wilber Site Sample 3 (Note: J_i is the initial distance from the nozzle to the soil surface) 59
Figure (35): Depth Gauge Reading vs. Time for Wilber Site Sample 4 (Note: J_i is the initial distance from the nozzle to the soil surface) 59
Figure (36): Depth Gauge Reading vs. Time for Hooper Site Sample 1 (Note: J_i is the initial distance from the nozzle to the soil surface) 60
Figure (37): Depth Gauge Reading vs. Time for Hooper Site Sample 2 (Note: J_i is the initial distance from the nozzle to the soil surface) 60
Figure (38): Depth Gauge Reading vs. Time for Hooper Site Sample 3 (Note: J_i is the initial distance from the nozzle to the soil surface) 61
Figure (39): Depth Gauge Reading vs. Time for Hooper Site Sample 4 (Note: J_i is the initial distance from the nozzle to the soil surface) 61
Figure (40): Depth Gauge Reading vs. Time for Beatrice Site Sample 1 (Note: J_i is the initial distance from the nozzle to the soil surface) 62
Figure (41): Depth Gauge Reading vs. Time for Beatrice Site Sample 2 (Note: J_i is the initial distance from the nozzle to the soil surface) 62
Figure (42): Depth Gauge Reading vs. Time for Beatrice Site Sample 3 (Note: J_i is the initial distance from the nozzle to the soil surface) 63
Figure (43): Depth Gauge Reading vs. Time for Beatrice Site Sample 4 (Note: J_i is the initial distance from the nozzle to the soil surface) 63
Figure (44): Depth Gauge Reading vs. Time for Beatrice Site Sample 5 (Note: J_i is the initial distance from the nozzle to the soil surface) 64
Figure (45): Depth Gauge Reading vs. Time for UNL City Campus Sample 1 (Note: J_i is the initial distance from the nozzle to the soil surface) 64
Figure (46): Depth Gauge Reading vs. Time for UNL City Campus Sample 2 (Note: J_i is the initial distance from the nozzle to the soil surface) 65
Figure (47): Depth Gauge Reading vs. Time for UNL East Campus Sample 1(Note: J_i is the initial distance from the nozzle to the soil surface) 65
Figure (48): Depth Gauge Reading vs. Time for UNL City Campus Sample 2 (Note: J_i is the initial distance from the nozzle to the soil surface) 66

List of Tables

Table (1) Summary of the Advantages and the Limitations for Each Testing Method.... 13
Table (2): Soil Properties Influencing the Erodibility of Cohesive Soils 21
Table (3): Correlations for Cohesionless Soils 22
Table (4): Correlations for Cohesive Soils 22
Table (5): Soil Properties 25
Table (6): Soil Classification 26
Table (7): Erosion Test results 31
Table (8): Erosion Categories (Briaud et al. 2017) 32
Table (9): Raw Test Data for Beatrice Location (S2) 34
Table (10): Input Parameters Used in the Calculation Procedure 35
Table (11): Calculations to Predict the Equilibrium Depth 36

Chapter 1

Introduction

1.1 Background

The erosion of riverbed soils under the bridges is considered one of the main causes of bridge failure (Briaud, 2015). According to Briaud & Hunt (2006), approximately 58 percent of bridge failures from 1966 to 2005 were due to erosion, based on the statistics calculated using the national bridge failure database collected by the Structures Division of NYSDOT. Similarly, in Nebraska, soil erosion is reported as a primary cause of bridge closure or failure (Kameshwar & Padgett, 2018), which substantially impacts the economy in general and particularly in agriculture and rural sectors (Nebraska Legislature Transportation & Telecommunications Committee, 2014). Nowadays, the prediction of soil erosion becomes more challenging with unpredictable weather patterns and unavoidable floods. In this context, it is essential to evaluate the erosion properties of the soils and accurately and conveniently estimate the field erosion that may be caused by flooding and heavy rain. However, the evaluation of this process is not straightforward due to the complexity of the hydrodynamic conditions that govern the erosion behavior of the soil, in addition to the wide varying erosion resistance of soils.

The experimental approach may be a logical way to obtain the soil's erosion properties. However, those processes are time-consuming and costly. Therefore, many empirical equations were presented in literature attempting to correlate the erosion resistance to the common soil properties. Obviously, the rational and empirical correlations may work more favorably in cohesionless soils than in cohesive soils. This is

because the erosion mechanism of the cohesionless soils is simple and depends mainly on the weight of the individual particles and the hydrodynamic forces around the particles.

On the other hand, the erosion behavior of cohesive soils is more complex. Many factors, such as water content, unit weight, plasticity index, void ratio, swelling pressure, mean grain size, soil and water temperature, undrained shear strength, percent fines, clay minerals, and other factors affect the erosion. This complexity leads to a high level of uncertainties and variation in the erosion properties of cohesive soils. Additionally, some erosion prediction software such as HEC-RAS and FLOW-3D-Hydro require the mean grain size as one of the major input parameters to compute the erodibility. The mean grain size diameter, however, may not properly model the erosion characteristics of cohesive soils. This leads to the idea of finding a simple equivalent sand particle diameter that can represent the erodibility of cohesive soils more realistically.

1.2 Research Objectives

This research aims to test and evaluate the critical shear stress and erodibility coefficient of Nebraska riverbed soils around Lincoln and obtain a simplified correlation providing the equivalent sand particle diameter for fine-grained soils that may be conveniently used in the analysis of soil. To achieve this goal, 17 samples from four different riverbeds were collected and tested with the Mini Jet Erosion Test (Mini-JET), aiming to:

- Determine the critical shear stress and the erodibility coefficient.
- Correlate the mean particle diameter to the critical shear stress.
- Obtain an equivalent sand particle mean diameter ($D_{50(\text{Sand Equivalent})}$) for the fine-grained soils that may provide easy and realistic erosion prediction.

Chapter 2

Literature review

In this chapter, a literature review was conducted on the general erosion mechanism, erosion testing methods, the difference between the erosion behavior of cohesive and cohesionless soils, and the existing correlations between the general soil properties and the erosion resistance.

2.1 Erosion Mechanism

In general, soil erosion is defined as a geological process of washing out and transporting soil particles due to the flowing water or wind effect (National Geographic, 2022). In many Civil Engineering applications, soil erosion occurs due to the flowing water. Briaud et al. (2004) defined the bridge scour as "soil loss by erosion due to water flowing around bridge supports."

Classical work for soil erosion was developed by Shields (1936) and that was known as the dimensionless erosion model. According to Buffington (1999), “Shields work on incipient motion and bed-load transport is a benchmark study that has inspired numerous investigations and is widely applied in fields”. Shields (1936) expressed the bed shear stress at the moment of sediment transport initiation in a dimensionless form as presented in Equation 1.

$$\tau_c^* = \frac{\tau_c}{(\rho_s - \rho)gD} \qquad \text{Equation 1}$$

where

τ_c^*: Dimensionless critical shear stress / Critical Shields’ parameter.

τ_c: Critical shear stress (Dimensional).

ρ_s: Sediment density.

ρ: Fluid density.

D: Characteristic grain size.

The idea of this model is that when the dimensionless bed shear stress exceeds the critical shield number, the erosion will occur. This model is still popular and used in soil erosion analysis software such as FLOW-3D-Hydro, particularly for course-grained soils.

Another common mathematical model that is used to describe the erosion process is known as the excess shear stress model or the dimensional model described in Equation 2. (Partheniades (1965), Hanson (1990a), Hanson (1990b), Hanson & Cook, (1997), Hanson & Cook (2004), Hanson & Hunt (2007), Simon et al., (2010), Al-Madhhachi et al., (2011), Al-Madhhachi et al., (2013), Khanal et al., (2016)).

$$\dot{\epsilon}_r = k_d(\tau_e - \tau_c)^a \qquad \text{Equation 2}$$

where

$\dot{\epsilon}_r$: Erosion rate (m/sec).

k_d: Erodibility coefficient (m^3/ N•sec).

τ_e: The fluid induced shear stress (Pa).

τ_c: Critical shear stress (Pa).

a: Empirical exponent which depends on the soil type.

The physical meaning of Equation 2 is that the erosion in the field occurs when the fluid-induced shear stress at the soil-water contact is higher than a threshold shear stress called the critical shear stress, and the erodibility coefficient governs the erosion rate. Therefore, two important behaviors should be considered when analyzing the erosion process; how deep the erosion will be and how fast the erosion will be. In other words, Equation 2 manifests that the critical shear stress represents the possible ultimate erosion depth, and the erodibility coefficient represents the erosion rate. In addition, the exponent (a) depends on the soil type; it is suggested to be 1 for cohesive soils and 1.5 for non-cohesive soils and has an upper limit of 2 (Stein et al. 1993). This leads to a dimensional trouble in the model when the exponent (a) is not equal to.

2.2 Testing Methods

Many devices are utilized to test and find the erodibility properties of different soil types. Some tests devices require remolding/preparing the sample, which may cause a disturbance, such as the Rotating Cylinder Test (RCT) (Moore & Masch 1962), while other tests may reduce the disturbance, such as the Erosion Function Apparatus (EFA) (Briaud et al. 1999) which push the Shelby tube samples directly into the erosion chamber. Additionally, some tests can be performed in the field, such as the submerged jets; Jet Erosion Test, and Mini Jet Erosion Test (Hanson & Cook 2004), (Simon et al. 2010). Finally, some tests are designed to mimic the large scale, such as The University of Mississippi Erosion Testing Bed (UMETB) (Song et al. 2011), (Jang et al. 2011). The procedures of these tests are presented in the following section.

2.2.1 Jet Erosion Test (JET)

Hanson & Cook (2004) developed the JET to estimate the soil erodibility in-situ, considering the submerged jet's hydraulic properties as well as soil erodibility properties. The main idea of submerged jets is to measure the scour depth caused by impinging water with time. The erosion begins when the shear stress induced by the fluid becomes larger than critical shear stress. As time goes on, the fluid-induced shear stress decreases as the erosion depth increases, leading to the equilibrium condition when the fluid-induced shear stress becomes less than soil resistance. Figure (1) shows a schematic of the apparatus. One main advantage of the submerged jets that they are portable and can be easily conducted in the laboratory or in the field.

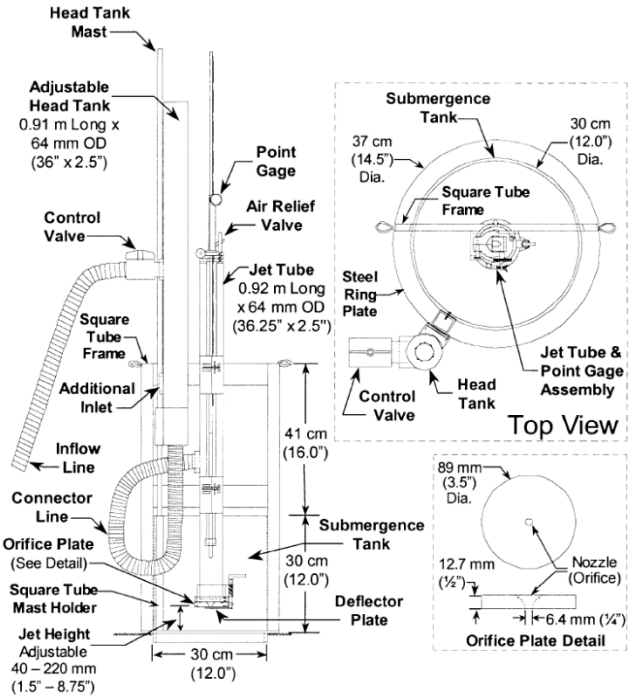

Figure (1): Schematic of JET by Hanson & Cook (2004)

The JET testing procedure is as follows based on Hanson & Cook (2004).

- Select the site considering the arrangement of the test apparatus, hoses, and pump.
- Drive the submergence tank into the soil surface.
- Assemble the jet tube and point gauge on the submersible's square tube frame.
- Attach the mast to the submergence tank's head tank mast holder and adjust the head tank height to the submergence tank's top.
- If a pump is utilized for water delivery, install it on the streambank or on a platform in the streambed to keep the engine dry.
- Connect hoses to the pump from the stream channel, the head tank from the pump, and the jet tube from the head tank.
- Determine the height of the jet nozzle using the point gauge.
- Set the point gauge against the deflector plate in front of the jet nozzle. This shuts the nozzle. Open the head tank and jet tube. An air release valve is located at the head of the jet tube.
- After filling the system with water, move the point gage more than ten nozzle diameters upstream of the jet nozzle to eliminate flow disruption.
- Ahead of filling the submergence tank, measure the distance between the top of the head tank and either the submergence tank or stream channel, whichever is higher. After that, move the deflector plate to begin testing. Take the head readings every 5 to 10 min.
- At specified time intervals, take point gauge measurements on the bed.

Using the time versus depth curve considering diffusion principles, the data can be reduced, and the shear stress parameters are obtained.

2.2.2 Mini Jet Erosion Test (Mini-JET)

This device is a miniature version of JET, which can make field tests easier. The Mini-JET was used firstly by Simon et al. (2010). Figure (2) presents the Mini-JET device.

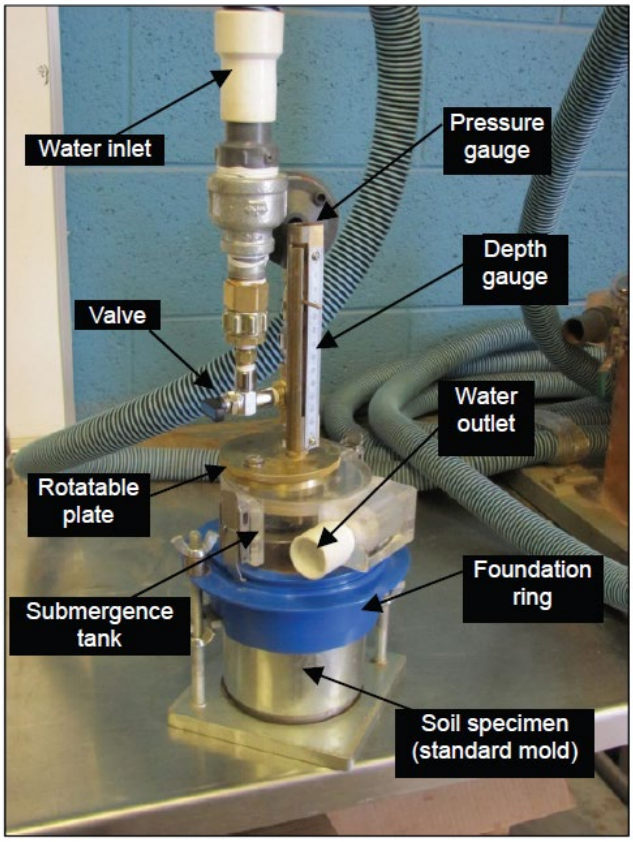

Figure (2): Mini JET Device by Al-Madhhachi et al. (2013)

The Mini-JET testing procedure is as follows based on Al-Madhhachi et al. (2013).

- Use the depth gauge to determine the height of the jet nozzle prior to turning on the water by taking depth gauge readings at the nozzle and the soil specimen surface at time zero.
- During the test, rotate the nozzle away from the impinging spot using the rotatable plate when the depth readings are taken.
- Close the jet valve and open the water supply to fill the head tank. Empty the adjustable head tank of all air following depth gauge readings.
- Open the jet valve to fill the submergence tank.
- Take the initial water head reading and keep it constant during the test.
- Rotate the nozzle to start the impingement of the sample and record the time.
- Take the depth readings at time intervals.

Using the time versus depth curve considering diffusion principles, the data can be reduced, and the shear stress parameters are obtained.

2.2.3 Erosion Function Apparatus (EFA)

Briaud et al. (1999) pioneered the idea of EFA to estimate the scour depth versus time beneath a cylindrical bridge pier of a specific diameter in clays. Then, it was used for different applications. One of the important advantages of this device is to reduce sample disturbance by taking samples using standard Shelby tubes.

Figure (3) shows a schematic for EFA.

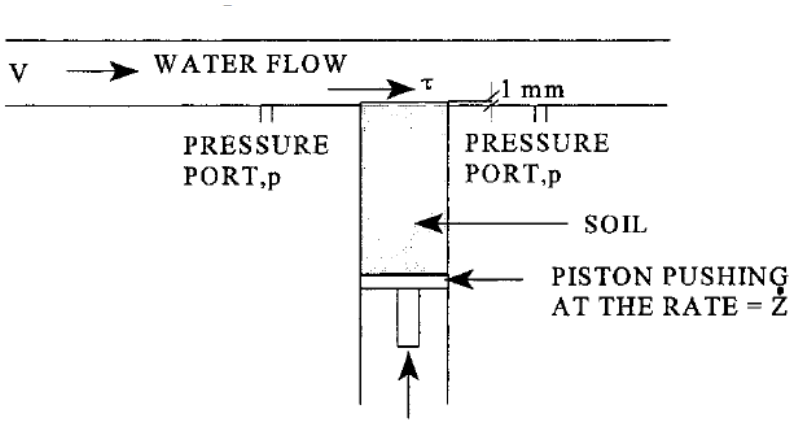

Figure (3): Schematic of EFA by Briaud et al. (1999)

The EFA testing procedure is as follows, excerpted from Briaud et al. (2001).

- "After inserting the sample into EFA, the pipe should be filled with water and left for an hour.
- The velocity should be set at 0.3 m/s.
- One millimeter of the soil sample should be extruded towards the flow.
- The required time to erode the one millimeter of the soil sample should be recorded.
- The velocity should be increased to 0.6 m/sec, and the sample should go back to the one-millimeter position either when the initial one millimeter of soil has been eroded or after an hour.
- Again, the required time to erode the one millimeter of the soil sample should be recorded.
- Finally, the previous two steps should be repeated velocities 1 m/s, 1.5 m/s, 2 m/s, 3 m/s, 4.5 m/s, and 6 m/s."

2.2.4 Rotating Cylinder Test (RCT)

The Rotating Cylinder Test was developed by Moore & Masch (1962). Then, some improvements were introduced by Chapuis & Gatien (1986). The main idea of RCT is to apply torque on an inner cylindrical soil sample by a generated shear stress induced by the fluid motion. The fluid motion is caused by the rotation of an outer cylinder.
The RCT testing procedure is as follows based on Chapuis & Gatien (1986).

- The clay cylinder should be fixed on a pivoting base and contained inside a transparent concentric cylinder that can be turned at a controlled speed of up to 1750 revolutions per minute.
- Water should be supplied into the annular space to determine its erosive properties.
- The rotating outer cylinder imparts rotation to the fluid, transferring shear to the surface of the clay cylinder, which is maintained stationary by a pulley-and-variable-weight system.
- Each test contains many stages performed at a steady rotational speed, and each stage lasts between 10 and 30 minutes.
- The shear stress-induced couple should be continuously recorded.
- The cell should be cleaned with fresh fluid.
- The eroded particles should be weighed after they dry.

The critical shear stress is computed using the torque recorded at the start of the erosion procedure. Then, the erosion rate is determined by the measuring weight at regular time intervals.

2.2.5 The University of Mississippi Erosion Testing Bed (UMETB)

The University of Mississippi Erosion Testing Bed was developed and used by Song et al. (2011), Jang et al. (2011) and Kidd et al. (2011) in order to mimic the erosion behavior of levee soils under a plunging two-dimensional water jet. Figure (4) shows the UMETB.

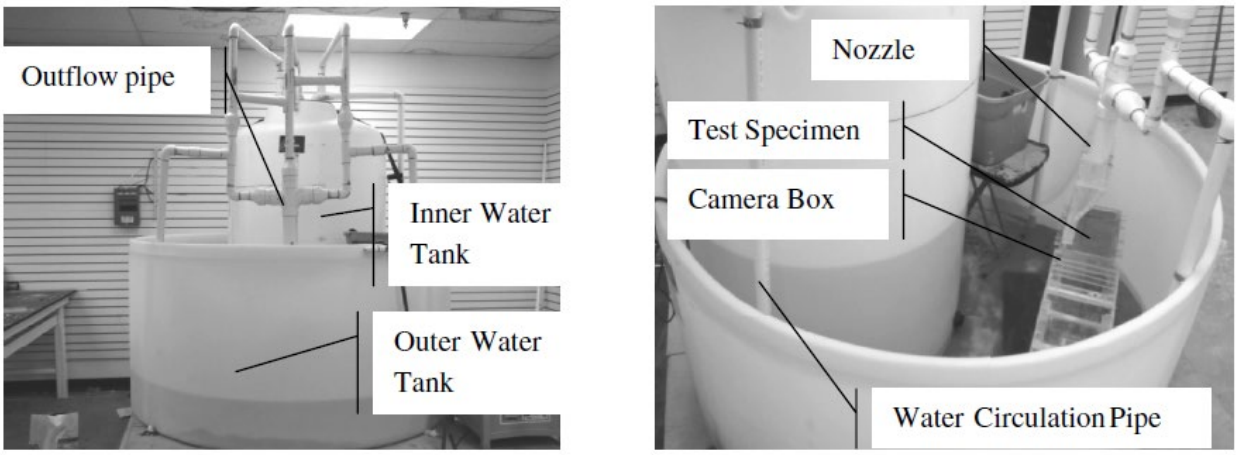

(a) (b)

Figure (4): a) View of outside UMETB, b) View of inside UMETB (Song et al. 2011).

The UMETB testing procedure is as follows based on Song et al. (2011).

- The dry soil sample should be placed and spread in the specimen box using a small shovel.
- Without disturbing the soil sample, water should be added slowly to saturate it.
- The specimen box should be placed on the test bench, and the nozzle height should be adjusted until the nozzle makes contact with the top of the flood wall and the water flows smoothly along the wall.
- The camera should be placed and adjusted manually to capture the erosion profile.
- All pumps should be turned on at the same time to supply water to the nozzle.

- The test box should be covered with a plate in order to achieve a constant flow rate before the erosion starts.

Each test has pros and cons. Table (1) summarize the advantages and the limitations for each test.

Table (1) Summary of the Advantages and the Limitations for Each Testing Method

Testing device	Advantages	Limitations
JET	Can be performed in the lab and in the field.	Cannot measure deep erosion.
Mini-JET	Easy to use and perform in both lab and field.	Any large particle (gravel for example) may cause a disturbance in the test.
EFA	Reduce the disturbance of the soil sample as it is taken using a standard Shelby tube.	Cannot be conducted in the field.
RCT	The shear stress can be derived directly from the torque.	The eroded particles will change the water density which leads to change in the shear stress.
UMETB	The testing procedure is easy. There is no need to stop the flow while taking the readings. Can accommodate large sample size.	It is basically dependent on image proccing. So, it is not easy to use it for cohesive soils when the erosion water is mucky.

2.3 Development of the Excess Shear Stress Parameters for Circular Jets.

2.3.1 Hanson & Cook (1997) Derivation

This part includes the derivation process of the excess shear stress parameter in the circular jets presented by Hanson & Cook (1997), which is used to analyze the test results of this study. In addition, it shows the main differences between Hanson & Cook (1997) derivation and Stein et al. (1993).

Hanson & Cook (1997) utilized the excess shear stress concept and develop it for circular jets. The derivation procedure is shown below.

The derivation starts with the commonly used procedure to calculate the erosion rate.

$$\epsilon_r = k_d(\tau_e - \tau_c)^a \qquad \text{Equation 2}$$

where,

ϵ_r: Erosion rate (m/sec).

k_d: Erodibility coefficient (m^3/ N•sec).

τ_e: Average hydraulic boundary shear stress/ Maximum stress caused by jet/ Interface shear stress (Pa).

τ_c: Critical shear stress (Pa).

a: Empirical exponent which depends on the soil type.

The velocity will be constant within a certain depth, which is called the potential core length. However, it will be decreased depending on the distance between the nozzle and the soil surface outside the potential core length. Hanson & Cook (1997) used the formulation presented by Albertson et al. (1950) to compute this velocity.

$$\frac{U}{U_o} = C_d \frac{d_o}{J}$$ Equation 3

where

U: Velocity outside the potential core length at any depth (J).

U_o Initial velocity at the nozzle.

C_d: Diffusion coefficient.

d_o: Nozzle diameter.

Using Equation 3, and considering that the flow velocity is equal to the initial velocity within the potential core length, the potential core length is written follows.

$$J_p = C_d d_o$$ Equation 4

The maximum shear stress on the bed in the impingement region is related to the maximum velocity and a friction coefficient.

$$\tau = C_f \rho U_o^2$$ Equation 5

Considering that the velocity is different inside and outside the potential core length, Equation 5 is written in two ways as follows.

$$\tau_o = C_f \rho U_o^2 \qquad \text{for } J \leq J_p$$ Equation 6

$$\tau = C_f \rho (C_d U_o \frac{d_o}{J})^2 \qquad \text{for } J > J_p \qquad \text{Equation 7}$$

Then, Equation 2 is rewritten as follows assuming that the martial constant (a) =1.

$$\frac{dJ}{dt} = k_d(\tau_o - \tau_c) \quad \text{for } J \leq J_p \qquad \text{Equation 8}$$

$$\frac{dJ}{dt} = k_d[C_f \rho \left(C_d U_o \frac{d_o}{J}\right)^2 - \tau_c] \quad \text{for } J > J_p \qquad \text{Equation 9}$$

Considering that $\tau_o = C_f \rho U_o^2$, and $J_p = C_d d_o$ Equation 9 is rewritten as follows.

$$\frac{dJ}{dt} = k_d[\tau_o \frac{J_p^2}{J^2} - \tau_c] \quad \text{for } J > J_p \qquad \text{Equation 10}$$

The equilibrium depth is defined as the scour/ erosion depth at which the fluid flow is unable to erode more soil particles. In other words, it occurs when the fluid induced shear stress is lower than the critical shear stress. Assuming that the equilibrium depth will occur at $\frac{dJ}{dt} = 0$. Then,

$$\frac{dJ}{dt} = k_d[\tau_o \frac{J_p^2}{J_e{}^2} - \tau_c] = 0$$

$$\tau_o \frac{J_p^2}{J_e{}^2} = \tau_c$$

$$\tau_c = \tau_o \left(\frac{J_p}{J_e}\right)^2 \qquad \text{Equation 11}$$

Introducing dimensionless form as follows.

$$J^* = \frac{J}{J_e} \qquad \text{Equation 12}$$

$$T^* = \frac{t}{T_r} \qquad \text{Equation 13}$$

where T_r is the reference time introduced by Stein et al. (1993) as follows.

$$T_r = \frac{J_e}{\tau_c K_d} \qquad \text{Equation 14}$$

By substituting Equation 12, Equation 13, and Equation 14 in Equation 8 and Equation 10. The following dimensionless form are obtained.

$$\frac{dJ^*}{dT^*} = \frac{J_p^{*2}}{1-J_p^{*2}} \qquad \text{for } J \leq J_p \qquad \text{Equation 15}$$

$$\frac{dJ^*}{dT^*} = \frac{J^{*2}}{1-J^{*2}} \qquad \text{for } J > J_p \qquad \text{Equation 16}$$

Integrating Equation 15 from zero to the potential core length.

$$\int_0^{T_p^*} dT^* = \int_0^{J_p^*} \frac{J_p^{*2}}{1-J_p^{*2}} dJ^*$$

$$T_p^* = J^{p*}\left[\frac{J_p^{*2}}{1-J_p^{*2}}\right] \qquad \text{Equation 17}$$

Integrating Equation 16 from the potential core length to the initial depth.

$$T_i^* - T_p^* = 0.5 \ln\left(\frac{1+J_i^*}{1-J_i^*}\right) - J_i^* - 0.5 \ln\left(\frac{1+J_p^*}{1-J_p^*}\right) + J_p^* \qquad \text{Equation 18}$$

Integrating Equation 16 from the initial depth to any depth.

$$T^* - T_i^* = 0.5 \ln\left(\frac{1+J^*}{1-J^*}\right) - J^* - 0.5 \ln\left(\frac{1+J_i^*}{1-J_i^*}\right) + J_i^* \qquad \text{Equation 19}$$

From Equation 19 and the definitions of the dimensionless time.

$$T_m = T_r \left[0.5 \ln\left(\frac{1+J^*}{1-J^*}\right) - J^* - 0.5 \ln\left(\frac{1+J_i^*}{1-J_i^*}\right) + J_i^*\right] \qquad \text{Equation 20}$$

where $T_m = t - t_i$

2.3.2 The main differences between Hanson & Cook (1997) and Stein et al. (1993) derivations.

Stein et al. (1993) utilized the excess shear stress concept and develop it for circular jets based on different equations from those used by Hanson & Cook (1997). The difference in the derivation started by using different equation for the velocity outside the potential core length.

Stein et al. (1993) used Rajaratnam (1976) formulation to compute this velocity.

$$\frac{U}{U_o} = C_d \sqrt{\frac{d_o}{J}} \qquad \text{Equation 21}$$

Which led to different equations for the potential core length and the critical shear stress as follows.

$$J_p = d_o C_d^2 \qquad \text{Equation 22}$$

$$\tau_c = \tau_o \frac{J_p}{J_e} \qquad \text{Equation 23}$$

As a result, the final form for the equation was different than Hanson & Cook (1997). The final form is presented as follows.

$$T^* - T_p^* = -J^* - \ln(1 - J^*) \Big|_{J_p^*}^{J^*} \qquad \text{Equation 24}$$

2.4 Prediction of the Equilibrium Erosion Depth

It is not always possible or practical to achieve the equilibrium depth in the testing procedures, especially for cohesive soils, because the procedure takes a long time. As a result, some techniques were used to predict the equilibrium depth using data for a limited time period. The idea behind these techniques is that erosion will not continue forever. Two of the existing techniques are presented below.

2.4.1 Blaisdell et al., (1981) Hyperbolic Technique

This technique was used by Hanson & Cook (1997) to predict the equilibrium depth. Equation 25 presents (Blaisdell et al., 1981) hyperbolic equation.

$$(f - f_o)^2 - x^2 = A^2 \qquad \text{Equation 25}$$

where A is the value for the semi-transverse and semi-conjugate axis of the hyperbola.

$$x = Log\left(\frac{U_o t}{d_o}\right)$$

$$f = Log\left(\frac{J}{d_o}\right) - x$$

$$f_o = Log\left(\frac{J_e}{d_o}\right)$$

From the test data, the actual values of (f) and (x) are determined at each time. To get the best fit of (f) value, the hyperbolic equation can be written as follows:

$$f = \pm\sqrt{A^2 + x^2} + f_o \qquad \text{Equation 26}$$

The values of A and f_o are determined using excel solver by minimizing the summation of the squared errors between actual f and predicted f. Then, the value of f_o is used to determine the equilibrium depth as follows.

$$J_e = d_o 10^{f_o} \qquad \text{Equation 27}$$

2.4.2 Duncan and Chang (1970) Hyperbolic Function

As presented in Song et al. (2018), a hyperbolic function was used by Duncan & Chang (1970) for the stress-strain relation. However, this equation may also be used for the erosion process as follows when the overall shape is a hyperbolic one.

$$J = \frac{t}{\alpha + \beta t} \qquad \text{Equation 28}$$

where α is the slope of the line in t/J versus t plot, and α is the Y-axis intercept.

2.5 Factors Affecting Erosion Behavior of Cohesionless and Cohesive Soils

The general erosion behavior is different for cohesionless and cohesive soils due to the difference in the erosion mechanism. For cohesionless soils, erosion occurs particle by particle. So, their erosion may occur by particles sliding or particles rolling (Briaud et al. 2001). In other words, erosion is governed mainly by the weight of the cohesionless particles.

On the other hand, cohesive soils may erode particle by particle or block by block. However, there are many soil properties that may additionally affect erosion. Table (2) presents the soil properties that may affect the erodibility as mentioned in NCHRP Report 516 by Briaud et al. (2004). However, it is acknowledged that the quantification of individual parameters is not fully understood or researched yet.

Table (2): Soil Properties Influencing the Erodibility of Cohesive Soils

When this parameter increases	Erodibility
Soil water content	unknown
Soil unit weight	decreases
Soil plasticity index	decreases
Soil undrained shear strength	increases
Soil void ratio	increases
Soil swell	increases
Soil mean grain size	unknown
Soil percent passing sieve #200	decreases
Soil clay minerals	unknown
Soil dispersion ratio	increases
Soil cation exchange capacity	unknown
Soil sodium absorption ratio	increases
Soil pH	unknown
Soil temperature	increases
Water temperature	increases
Water chemical composition	unknown

2.6 Existing correlations

Many trials are presented in the literature to correlate the critical shear stress to the common soil properties. Briaud et al., (2017) summarized some of the correlations as follows based on his comprehensive research. However, it is acknowledged that these correlations are not perfect, and the behavior may be different depending on the location and soil conditions.

2.6.1 For course-grained soils

Table (3): Correlations for Cohesionless Soils

Correlation	R^2
$\tau_c = 2.507 \times 10^{-12} \times (\gamma^{3.931})(PF^{4.382})$	0.5
$\tau_c = 0.978 \times (WC^{-2.306})(PF^{1.991})$	0.7

Note: PF (%) = percent finer than the No. 200 sieve; WC (%) = water content.

2.6.2 For Fine-grained soils

Table (4): Correlations for Cohesive Soils

Correlation	R^2
$\tau_c = 3.347 \times 10^{-10} \times (PI^{-1.855})(d_{50}^{-1.05})(WC^{6.707})$	0.72
$\tau_c = 2.28 \times 10^{-15} \times (PI^{-1.732})(WC^{3.106})(PF^{6.412})$	0.6
$\tau_c = 1.354 \times 10^{-7} \times (PL^{0.666})(d_{50}^{-0.189})(WC^{4.046})$	0.5

Note: d_{50} (mm) = mean particle size; PF (%) = percent finer than the No. 200 sieve; PL (%) = plastic limit; WC (%) = water content.

Chapter 3

Sampling, Soil properties, Applied Testing Methods

3.1 Locations

A total of 21 erosion tests were conducted. Seventeen soil samples were taken from four different riverbeds in Nebraska; Maple Creek, Haines Branch, Big Blue, and Turkey Creek crossing four different bridges in Hooper, Lincoln, Beatrice, and Wilber, respectively. In Addition, four samples were taken from the University of Nebraska-Lincoln campuses in order to compare the behavior of submerged soils and non-submerged ones.

The exact locations of the samples are presented below, and Figure (5) presents a map of the approximate locations.

- Lincoln: 40.76745572464669, -96.79659787296681
- Wilber: 40.480247310523644, -97.01307438430149
- Hooper: 41.56124947702843, -96.54106570811922
- Beatrice: 40.25616620666122, -96.74659683928448
- Lincoln (City Campus): 40.829722, -96.656349
- Lincoln (East Campus): 40.821569, -96.688980

The average flow rates of the rivers crossing Lincoln, Wilber, Hooper, and Beatrice are 33.5 m^3/sec, 6.7 m^3/sec, 120 m^3/sec, and 53.8 m^3/sec respectively, and the peak flow rates are 143 m^3/sec, 934.5 m^3/sec, 991.1 m^3/sec, and 1560.3 m^3/sec, respectively.

Figure (5): Approximate Test Locations

3.2 Sampling Procedure and Samples Preparation

The samples were taken from the riverbeds to the lab using PVC caps. First, the caps were pushed into the riverbed and flipped carefully to collect the soil. The main purpose of this procedure is to reduce the disturbance of the soil as much as possible. After that, the samples were submerged in the water for a before conducting the erosion test to ensure that the condition is similar to the field condition. Figure (6) shows two sandy and clayey soil examples after the saturation process and before the erosion test.

Figure (6): Soil Samples Before the Erosion Test

3.3 Soil Properties

To classify the soil samples, the following tests were conducted based on Das (2015):

- ASTM: Standard D-2216: Determination of Water Content.
- ASTM Standard D-422: Sieve Analysis.
- ASTM Standard D-422: Hydrometer Analysis.
- ASTM Standard D-4318: Liquid Limit (Test-Percussion Cup Method).
- ASTM Standard D-4318: Plastic Limit.
- ASTM Standard D-2974: Determination of Organic Content.

Then, soil samples were classified based on the Unified Soil Classification System (USCS). Soil properties and classification are shown in Table (5) and Table (6). In Addition, the gradation curves are presented in Appendix A.

Table (5): Soil Properties

Site	Sample #	Water Content %	Organic Content %	LL	PL	PI	C_c *	C_u *
Lincoln	S1	44.3	5.1	35.1	20.3	14.8	-	-
	S2	33.8	5.3	30.6	19.4	11.2	-	-
	S3	35.6	5.1	35.1	20.3	14.8	-	-
	S4	49.2	5.1	35.1	20.3	14.8	-	-
Wilber	S1	46.8	2.1	36.8	22	14.8	-	-
	S2	52.6	3.5	43.4	24.7	18.7	-	-
	S3	13.9	-	NP	NP	NP	0.694	4
	S4	13.5	-	NP	NP	NP	0.756	6.07
Hooper	S1	52.5	2.8	27.3	25.5	1.5	-	-
	S2	36.0	2.7	23.8	21.7	2.1	-	-
	S3	18.0	-	NP	NP	NP	0.858	2.5
	S4	33.4	2.6	26.7	22.2	4.5	-	-
Beatrice	S1	20.4	-	NA	NA	NA	0.762	2.679
	S2	42.2	5.1	34.9	26.9	8	-	-
	S3	10.9	-	NP	NP	NP	2.813	1.25
	S4	49.3	4.7	24.3	17.5	6.8	-	-
	S5	48.9	1.2	35.3	26.6	8.7	-	-
UNL City Campus	S1	21.7	-	48.8	31.9	16.9	-	-
	S2	15.1	-	47.7	33.0	14.7	-	-
UNL East Campus	S1	20.1	-	42.0	24.7	17.3	-	-
	S2	21.1	-	42.3	25.01	17.29	-	-

*: C_c: Coefficient of gradation, and C_u: Coefficient of uniformity

Table (6): Soil Classification

Site	Sample #	Passing #200	% Silt	% Clay	D_{50} (mm)	Symbol	Name
Lincoln	S1	46	28	18	0.0867	SC	Clayey Sand
	S2	46	28	18	0.0867	SC	Clayey Sand
	S3	35	25	10	0.183	SC	Clayey Sand
	S4	46	28	18	0.0867	SC	Clayey Sand
Wilber	S1	65	49	16	0.0371	CL	Sandy Lean Clay
	S2	36	20	16	0.425	SC	Clayey Sand
	S3	0.6	-	-	0.842	SP	Poorly Graded Sand
	S4	1.75	-	-	1.35	SP	Poorly Graded Sand
Hooper	S1	64	59	5	0.057	ML	Sandy Silt
	S2	52	48	4	0.073	ML	Sandy Silt
	S3	0.7	-	-	0.57	SP	Poorly Graded Sand
	S4	54	48	6	0.069	ML	Sandy Silt
Beatrice	S1	0.6	-	-	0.61	SP	Poorly Graded Sand
	S2	76	63	13	0.0408	ML	Silt with Sand
	S3	0.1	-	-	1.28	SP	Poorly Graded Sand
	S4	59	50	9	0.073	CL-ML	Sandy Silty Clay
	S5	52	36	16	0.0368	ML	Silt with Sand
UNL City Campus	S1	29	22	7	0.39	SM	Silty Sand
	S2	19	14	5	0.688	SM	Silty Sand
UNL East Campus	S1	50	32	18	0.0745	CL	Sandy Lean Clay
	S2	48	26	22	0.048	CL	Sandy Lean Clay

In general, the riverbed soils were shallow underwater sediments. They seemed to be young soils that did not develop strong bonding or interlocking system yet. Soils in Lincoln site seemed about the same type (mix between coarse and fine soils) on all sides around the bridge. They seemed very weak, especially after submergence, which may indicate that they contain a high percent of expansive minerals. On the other hand, different soil types were observed in Hooper, Wilber, and Beatrice; some parts around these bridges seemed to be pure sandy soil, and others contained either fine soils or mixed between fine soils and sand. In particular, soils in Beatrice showed a wide variety of soil types from pure sand, sticky fine soils, and a mix between fine soils and sand. This is expected because Beatrice bridge is a large bridge and has a high flow rate and low flow rate depending on the location.

Soils obtained from the UNL campus were not riverbed soils. In other words, they are not new fresh deposits, and they were tested with their natural moisture content without one day submergence period.

3.4 Testing Method and Analysis Procedure

In this study, the Mini-JET device described in section 2.3.2 was used to predict the erodibility properties. In addition, the analysis procedure considers the following.

- The equations were applied based on Hanson & Cook (1997) derivation as described in section 2.3.1.
- The prediction of the equilibrium depth was based on Duncan and Chang (1970) as described in section 2.4.2. when needed (Most of the samples reached the equilibrium depth during the test).

In addition, the Blaisdell et al. (1981) solution was used to predict the equilibrium depth and it turns that it gave close values to Duncan and Chang (1970). However, some constraints were applied to the solver to get reliable results. The GRG-Nonlinear solver was used on Excel with an upper limit of f_o. This procedure was used to check if there is a substantial difference between the equilibrium depth prediction techniques. (Results from Blaisdell et al. (1981) solution are not included in the thesis).

Chapter 4

Test Results and Discussion

4.1 Erosion Plots

The Mini JET was used to plot the erosion versus time plot for all samples, and the plot was used to predict the excess shear stress parameters. Figures (7) through (11) present the plots.

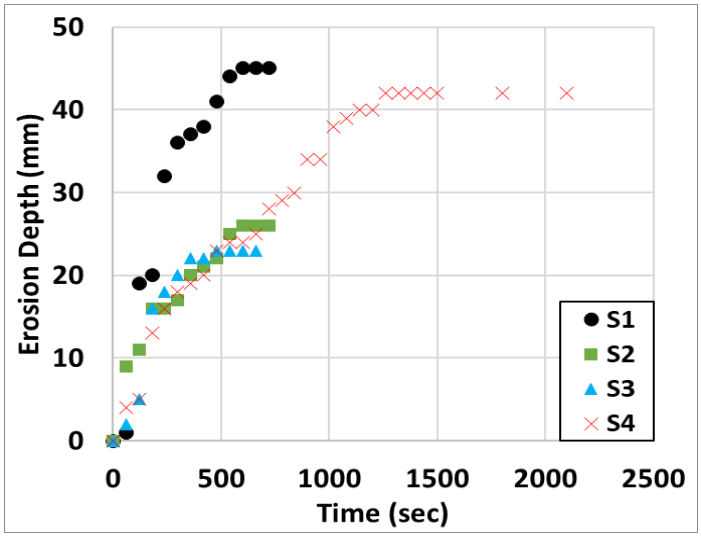

Figure (7): Erosion vs. Time for Lincoln Site (Note: Sample's names are matched to these in Table (5).)

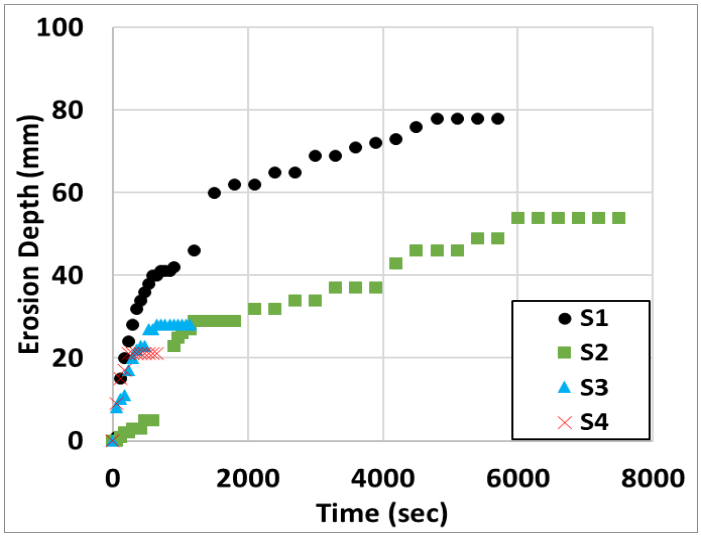

Figure (8): Erosion vs. Time for Wilber Site (Note: Sample's names are matched to these in Table (5).)

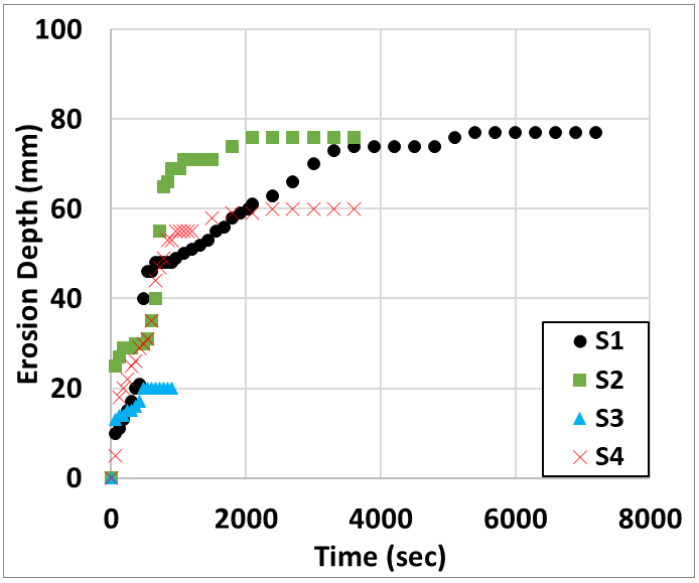

Figure (9): Erosion vs. Time for Hooper Site (Note: Sample's names are matched to these in Table (5).)

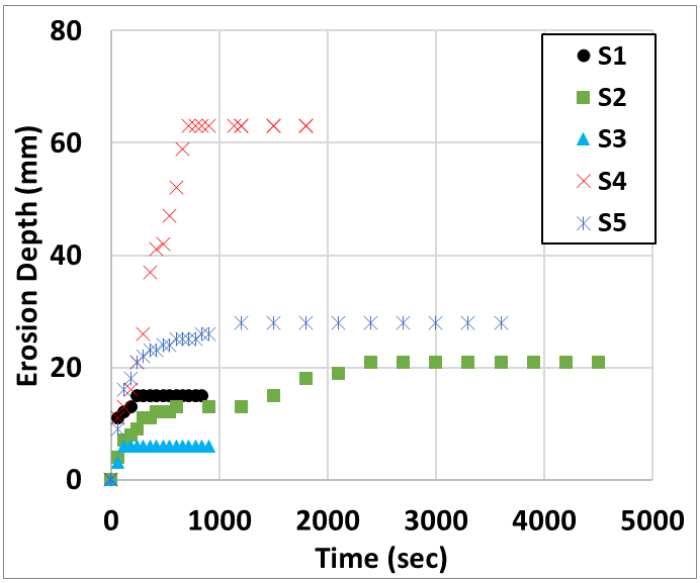

Figure (10): Erosion vs. Time for Beatrice Site (Note: Sample's names are matched to these in Table (5).)

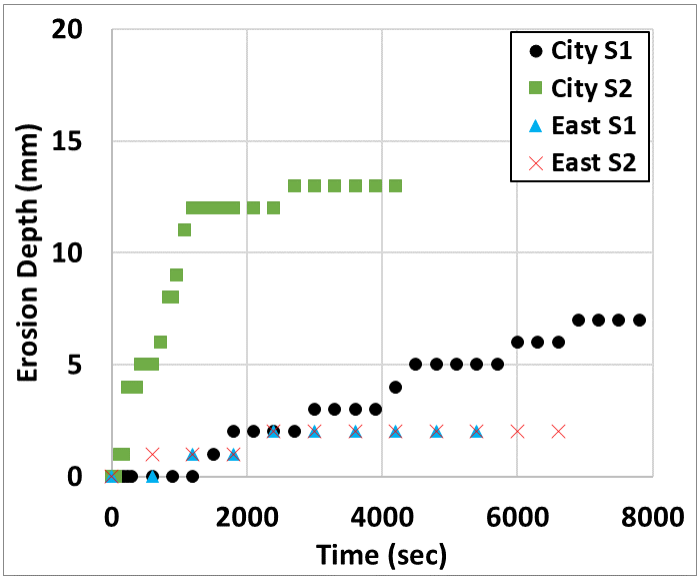

Figure (11): Erosion vs. Time for UNL Campuses (Note: Sample's names are matched to these in Table (5).)

The erosion curves show a wide variety in the erosion behavior of soils depending on the locations and even in the same location. The equilibrium erosion depth varies from 2 mm to around 80 mm, indicating a wide range of critical shear stress. In addition, the shape of the curves indicates the erodibility coefficient. The curves show the highest critical shear stress in the samples from the UNL campuses, which is expected because the samples are not riverbed soils. However, lower critical shear stress is observed for some samples in Hooper and Wilber locations. In addition, some curves show different fragmented curves, such as S2 in Wilber, S2, and S4 in Wilber, and S2, and S4 in Beatrice, presumably indicating layered soils' behavior sourced from the seasonal fluctuation of the river level – fine particles are sedimented during the period of low water level while coarse particles are sedimented during the period of high water level.

In this case, the excess shear stress parameters were obtained to get the best fit for the overall erosion curve.

4.2 Critical Shear Stress and Erodibility Coefficient

To find the magnitude of the critical shear stress and the erodibility coefficient, Hanson & Cook, (1997) method described in section 2.3.1 was used.

4.2.1 Magnitude of Excess Shear Stress Parameters

The testing results of Mini-JET for soil from six sites are summarized in Table (7).

Table (7): Erosion Test results

Site	Sample #	J_e (m)	τ_c (Pa)	k_d (cm^3/N•sec)	USCS Symbol
Lincoln	S1	0.1116	1.36	101.63	SC
	S2	0.0881	2.18	63.17	SC
	S3	0.0699	3.45	32.46	SC
	S4	0.1097	1.41	39.44	SC
Wilber	S1	0.1222	1.13	20.31	CL
	S2	0.0911	2.04	5.36	SC
	S3	0.0729	3.18	24.14	SP
	S4	0.0651	3.99	47.23	SP
Hooper	S1	0.1184	1.21	15.4	ML
	S2	0.1187	1.2	44.17	ML
	S3	0.0613	4.5	23.5	SP
	S4	0.1002	1.69	21.17	ML
Beatrice	S1	0.0553	5.52	32.35	SP
	S2	0.0592	4.83	4.42	ML
	S3	0.0461	7.95	25	SP
	S4	0.1147	1.29	49.89	CL-ML
	S5	0.0658	3.91	12.01	ML
UNL City Campus	S1	0.0421	9.55	0.42	SM
	S2	0.049	7.02	2.66	SM
UNL East Campus	S1	0.0383	11.54	0.96	CL
	S2	0.0392	11	1.06	CL

In terms of the critical shear stress, and based on the threshold values expressed by Briaud et al. (2017) shown in Table (8), the tested soils show the range between high erodibility geomaterials to low erodibility geomaterials. However, most samples were in the medium erodibility geomaterials range.

Table (8): Erosion Categories (Briaud et al. 2017)

Erosion Category	Description	Critical Shear Stress (Pa)	Critical Velocity (m/sec)
I	Very-high-erodibility geomaterials	0.1	0.1
II	High-erodibility geomaterials	0.2	0.2
III	Medium-erodibility geomaterials	1.3	0.5
IV	Low-erodibility geomaterials	9.3	1.35
V	Very-low-erodibility geomaterials	62	3.5
VI	Nonerosive materials	500	10

In terms of the erodibility coefficient, it was noticed that the values are high for these riverbed soils. To compare the results with Briaud et al. (2017), the erosion rates (mm/h) for all samples were calculated based on Equation 2, assuming that the empirical parameter (a) is equal to 1. Then, the test results were plotted on the erosion charts by Briaud et al. (2017) as presented in Figure 12. When the erosion rate was combined with the critical shear stress, the classification of the riverbed soils was shifted to the high erodibility geomaterials range.

To ensure that the testing device is giving reliable parameters, four samples were taken from the UNL campus and tested under different conditions; without submerging them under water for one day. With this condition, it is expected that the samples will erode

slower than the riverbed soils. The test results were as expected; the critical shear stress was in the range of 7.02 – 11.54 Pa. The erodibility coefficient was in the range of 0.42 to 2.66 $cm^3/N•sec$, indicating that the testing device is giving reliable results. According to Briaud et al. (2017) classification, and based on Table 8, these soils from UNL campus were in the range of low erodibility geomaterials. However, when combining the erosion rate with the critical shear stress, the classification shifts to the medium erodibility geomaterials range as shown in Figure 12.

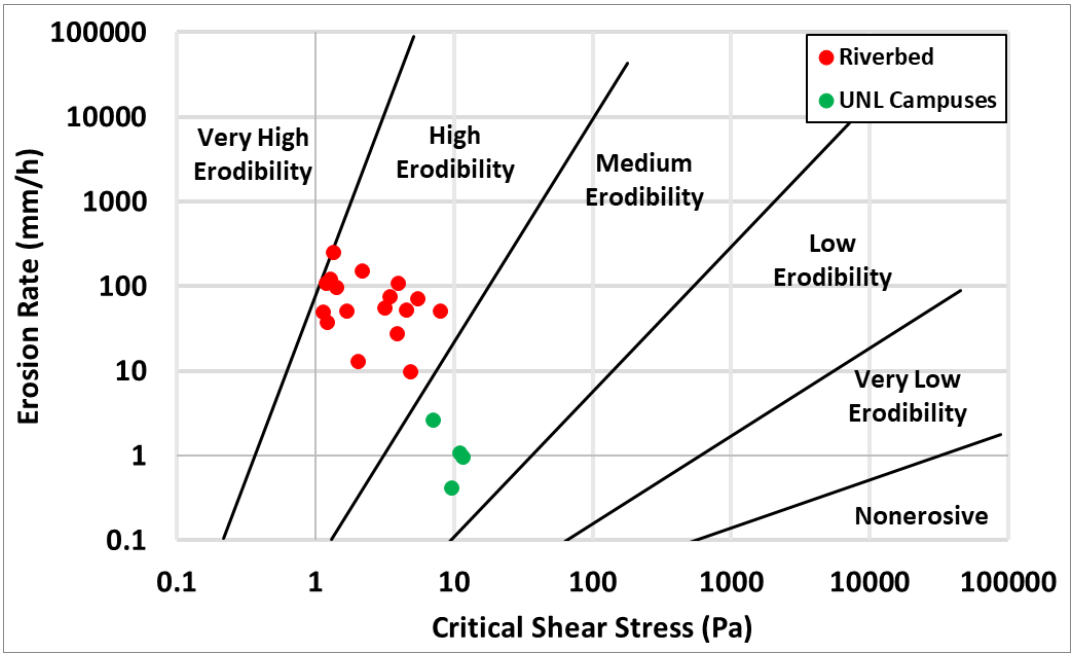

Figure (12): Erosion Charts by Briaud et al. (2017)

From the significant difference in the erosion behavior of Hooper soils and UNL East Campus soils even when both have about the same particle size, it is believed that particle size itself may not solely govern the erosion behavior. Instead, fully submerged and preferably dispersed soils may contribute a lot lower erosion resistance.

4.2.2 Sample Calculation for Beatrice S2 Sample

The raw test data is presented in Table (9).

Table (9): Raw Test Data for Beatrice Location (S2)

Time (sec)	Reading (m)
0	0.037
60	0.041
120	0.044
180	0.045
240	0.046
300	0.048
360	0.048
420	0.049
480	0.049
540	0.049
600	0.05
900	0.05
1200	0.05
1500	0.052
1800	0.055
2100	0.056
2400	0.058
2700	0.058
3000	0.058
3300	0.058
3600	0.058
3900	0.058
4200	0.058
4500	0.058

The input parameters which used to calculate the velocity of the water, the potential core length, and the fluid induced shear stress are summarized in Table (10).

Table (10): Input Parameters Used in the Calculation Procedure

Parameter	Magnitude	Unit	Reference
Density of water	1000	Kg/m^3	
Diameter of nozzle	0.00318	m	(Al-Madhhachi et al. 2013)
Diffusion coefficient	6.3	-	(Al-Madhhachi et al.2013)
Head	0.914	m	(Al-Madhhachi et al. 2013)
Friction coefficient	0.00416	-	(Al-Madhhachi et al. 2013)
Discharge coefficient	0.75	-	(Al-Madhhachi et al. 2013)

Then, the maximum velocity which is the velocity at the jet nozzle is computed as follows based on Hanson and Cook (2004) and Al-Madhhachi et al. (2013).

$$U_o = C\sqrt{2gh} \qquad \text{Equation 29}$$

where,

C: Discharge coefficient (0.7-0.75) for the Mini-JET and 1 for the original JET. (Al-Madhhachi et al., 2013).

g: Gravitational acceleration 9.81 m/sec^2

h: head in cm (0.91 m) (Al-Madhhachi et al., 2013)

Then, $U_o = 0.75\sqrt{2 * 9.81 * 0.9} = 3.18\, m/sec$

Al-Madhhachi et al. (2013) defined the discharge coefficient as the slope of the plotted measured discharge data versus $A\sqrt{2gh}$ based on the equation $Q = CA\sqrt{2gh}$ such that (h) is the applied water head, Q is the measured discharge, and A is the nozzle area.

The potential core length is calculated based on Equation (4) as follows.

$$J_p = C_d d_o = 6.3 * 0.00318 = 0.020034\, m.$$

The fluid induced shear stress is given by Equation (6) as follows.

$$\tau_o = 0.00414 * 1000 * 3.18^2 = 41.97\ Pa$$

The equilibrium depth prediction is conducted based on the hyperbolic technique by Duncan and Chang (1970). The calculations to obtain the t/*J* vs t curve is presented in Table (11), and the t/*J* vs t curve is plotted in Figure (13).

Table (11): Calculations to Predict the Equilibrium Depth

Time (sec)	Test reading (m)	Erosion reading (m)	t/*J*
0	0.037	0	-
60	0.041	0.004	15000
120	0.044	0.007	17142.85714
180	0.045	0.008	22500
240	0.046	0.009	26666.66667
300	0.048	0.011	27272.72727
360	0.048	0.011	32727.27273
420	0.049	0.012	35000
480	0.049	0.012	40000
540	0.049	0.012	45000
600	0.05	0.013	46153.84615
900	0.05	0.013	69230.76923
1200	0.05	0.013	92307.69231
1500	0.052	0.015	100000
1800	0.055	0.018	100000
2100	0.056	0.019	110526.3158
2400	0.058	0.021	114285.7143
2700	0.058	0.021	128571.4286
3000	0.058	0.021	142857.1429
3300	0.058	0.021	157142.8571
3600	0.058	0.021	171428.5714
3900	0.058	0.021	185714.2857
4200	0.058	0.021	200000
4500	0.058	0.021	214285.7143

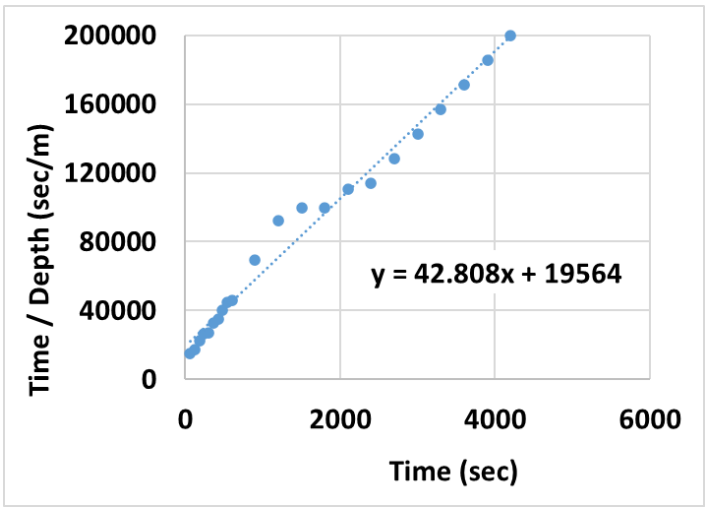

Figure (13): Duncan and Chang (1970) Hyperbolic Curve

To check how this technique fits the data, the erosion curve is plotted based on the equation obtained from Figure (13) as follows and presented in Figure (14).

$$J(m) = \frac{t(\text{sec})}{42.808t + 19564}$$

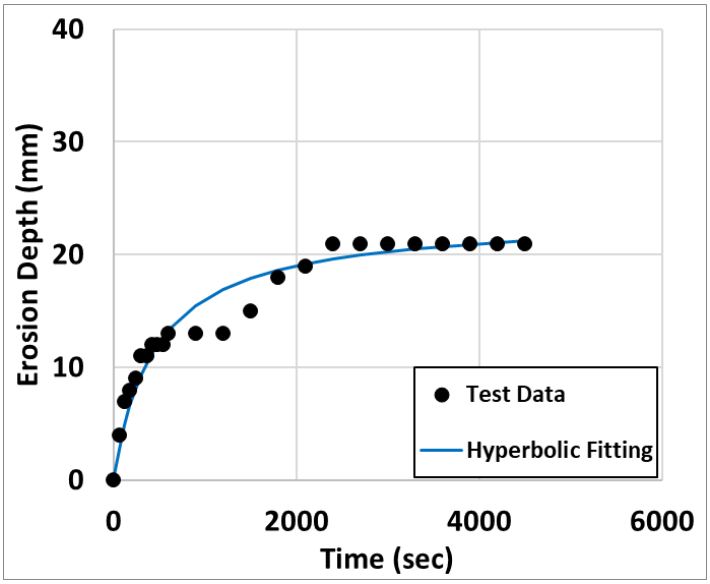

Figure (14): Actual Test Data and Predicted Data Based on Duncan and Chang (1970)

It is obvious that the sample has two layers. Then, there is a possibility of plotting two curves. However, the excess shear stress parameters were obtained based on one best fit curve as explained in section 4.1.

From Figure (14), the maximum erosion depth (for t = ∞) is 1/slope of the line = 1/ 42.808 = 0.0234 m.

In this calculation, the initial depth is not considered. So, the initial depth should be added to get the equilibrium depth.

$$J_e = 0.0234 + 0.037 = 0.0604 \text{ m}$$

Based on Equation (13), the critical stress is calculated as follows.

$$\tau_c = \tau_o \left(\frac{J_p}{J_e}\right)^2 = 41.97 * \left(\frac{0.020034}{0.0604}\right)^2 = 4.62\ Pa$$

According to Hanson & Cook (2004), Equation 22 is used to predict the erodibility coefficient. Equation 20 is rewritten using the definition of the reference time as follows.

$$T_m = \frac{J_e}{\tau_c K_d}\left[0.5 \ln\left(\frac{1+J^*}{1-J^*}\right) - J^* - 0.5 \ln\left(\frac{1+J_i^*}{1-J_i^*}\right) + J_i^*\right] \qquad \text{Equation 30}$$

Using the Excel solver with the testing data and predetermined critical shear stress, K_d is determined by reducing the error squared.

$$K_d = 3.48\ cm^3/N \cdot sec$$

In order to double check that the obtained excess shear stress parameters are representative for the erosion behavior of the soil. Equation 20 is rewritten as

$$2\frac{T_m}{T_r} + \ln\left(\frac{1+J_i^*}{1-J_i^*}\right) - 2J_p^* = \ln\left(\frac{1+J^*}{1-J^*}\right) - 2J^* \qquad \text{Equation 31}$$

At any time, the left side of the equation is known. So, the equation is solved for one unknown which is J* based on the calculated parameters and the erosion profile is plotted as shown in Figure (15). Appendix B includes the raw testing data and the back calculated data for all samples.

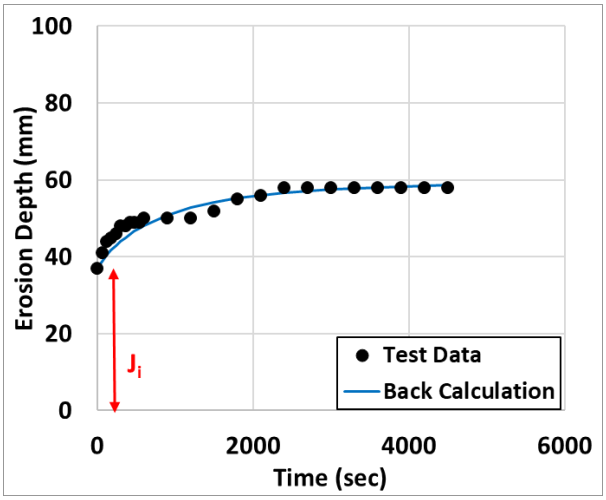

Figure (15): Test Data vs. Back Calculated Data (Note: J_i is the initial distance from the nozzle to the soil surface)

The plot shows a good match between the back calculated data and the original data which indicates that the obtained excess shear stress parameters are representative. The erosion profiles with the back calculated data are presented in Appendix B.

4.3 Comparison with Previous Research

4.3.1 Comparison with Hanson & Simon (2001)

A study was conducted by Hanson & Simon (2001) on the cohesive streambeds in the midwestern area of the US. Particularly Western Iowa, Eastern Nebraska, and Yalobusha River Basin, Mississippi. Figure (16) shows the data from Hanson & Simon (2001) in addition to the data from the current study.

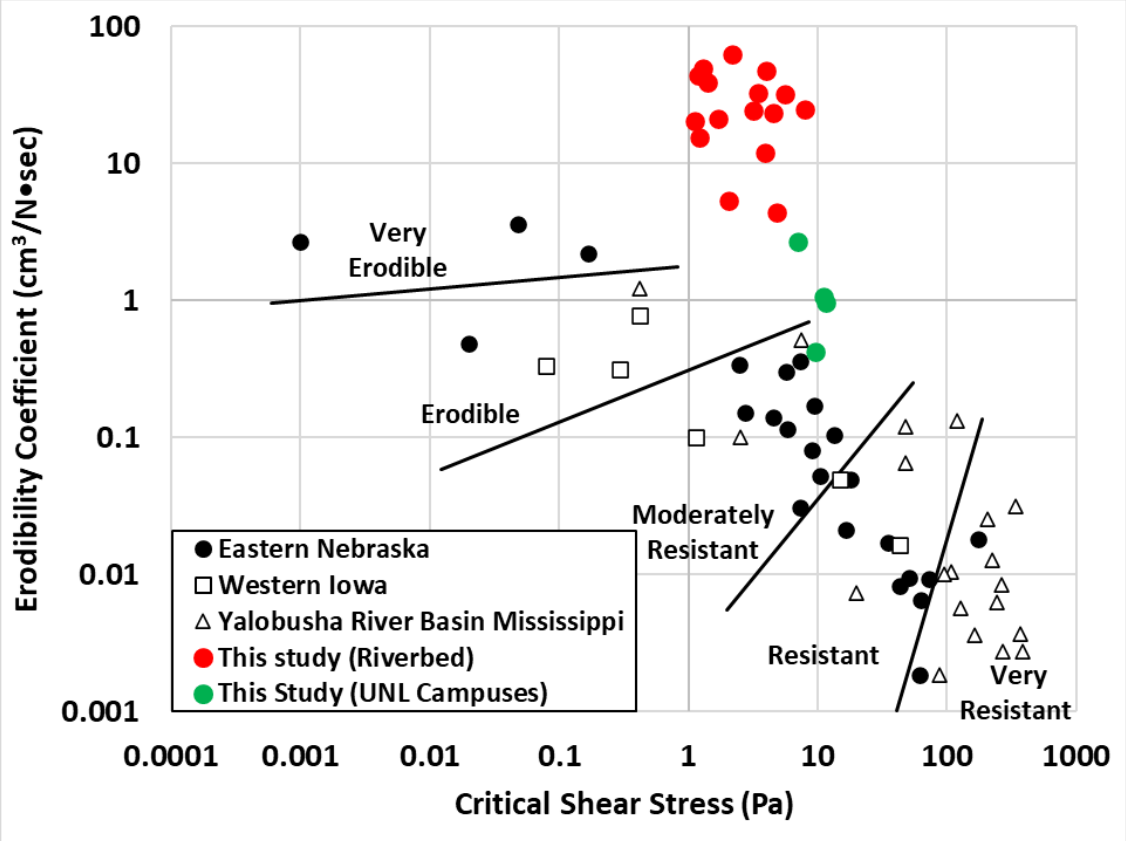

Figure (16): Critical Shear Stress vs. Erodibility Coefficient Based on Hanson and Simon (2001)

Figure (16) shows that there is a good match between this study and Hanson & Simon (2001) in terms of the critical shear stress. However, the erodibility coefficient is about

one order higher. It is thought that this difference may be caused by the difference in the soil types and testing conditions.

Even in Eastern Nebraska, there are a wide variety of soil types that may have different erosion resistance. It is believed that the tested soils may have a high percentage of expansive minerals (smectite), leading to low erosion resistance.

Also, the soil condition has a significant role in the erosion resistance; if the soils were submerged in water for a long time, the cohesion effect might be negligible at the shallow depth. This effect is clear comparing the riverbed soils with the UNL campus soils.

In general, the overall erosion behavior of the tested soils is that they may erode faster than the soils from the previous study due to the high erosion coefficient but to about the same depth due to the similar critical shear stress.

4.3.2 Comparison with Simon et al. (2010)

To double-check that the results are not out of the range, the test results were compared with other research conducted by Simon et al. (2010) that contains 279 samples tested using the Mini-JET. Figure (17) presents the results of this study superimposed to Simon et al. (2010) replotted data. The data points in this study are within Simon et al. (2010) range. However, the soils have a higher erodibility coefficient at the similar critical shear stress.

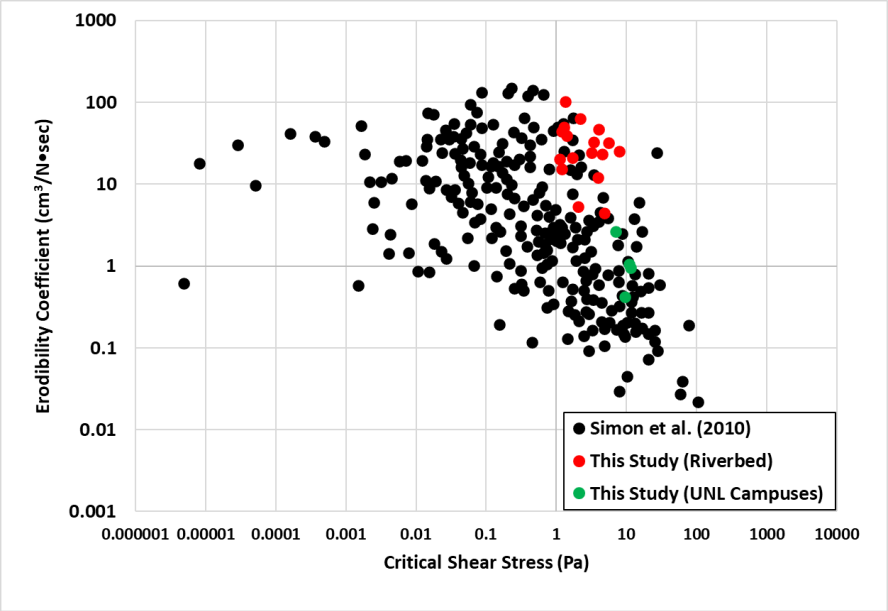

Figure (17): Critical Shear Stress vs. Erodibility Coefficient Based on Simon et al. (2010) with Test Results in This Study

4.3.3 Comparison with Briaud et al. (2017)

The mean grain size D_{50} vs. the critical shear stress was already plotted in previous research conducted by Briaud et al. (2017). Briaud et al. (2017) combined their study with TAMU data reported previously in (Briaud et al. (2001), and Seed et al. 2006)), in addition to the data by (Shields (1936), Gilbert (1914), USACE (1936), Casey (1935), and White 1940), Considering the objectives of this research, the testing results in this study were superimposed on the previous plot and presented in Figure (18).

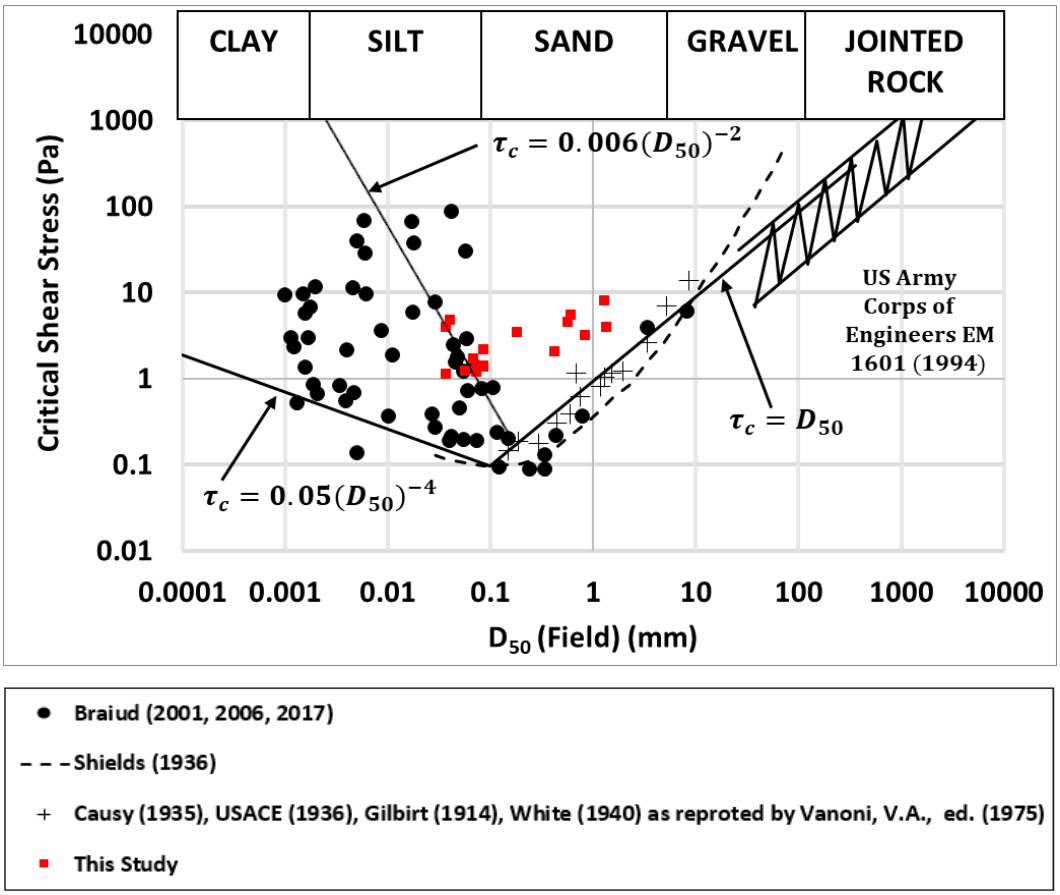

Figure (18): Mean Grain Size D_{50} vs. Critical Shear Stress (Replotted from Briaud et al. (2017))

The data points by Briaud et al. (2017) may be interpreted such that the critical shear stress is linearly proportional to the mean grain size for soils with diameter larger than 0.2 mm. However, the case is different for soil with diameter smaller than 0.2 mm. This difference is believed to be due to several factors, such as cohesion, plasticity index, void ratio, fine's percent, dispersion characteristics, soil temperature, water temperature, etc. as discussed in Table (2).

Comparing the test results of this study with Briaud et al. (2017), the samples with D_{50} > 0.2 mm show a slightly higher critical shear stress (τ_c). On the other hand, the samples with D_{50} < 0.2 mm show about the same erosion resistance (τ_c) as the upper limit of the previous study. This similarity can validate the upper limit equation given by Briaud et al. (2017) for the silty soils around Lincoln.

Based on this finding, one can predict an equivalent sand particle for the fine-grained soils around Lincoln, Nebraska in a way that will provide a reliable critical shear stress (τ_c) without underestimation using the following procedure.

If a silty soil sample around Lincoln, Nebraska has an actual diameter of $D_{50(Field)}$, which is obtained using the gradation analysis (sieve analysis and hydrometer analysis). Then, the equivalent diameter $D_{50(Sand\ Equivalent)}$ can predicted by considering the critical shear stress in $\tau_c = D_{50(Field)}$ equal to the critical shear stress in $\tau_c = 0.006(D_{50(Field)})^{-2}$. As a result, the equivalent diameter is given by Equation 32, and Figure (19) presents the concept behind the derivation.

$$D_{50(Sand\ Equivalent,\ mm)} = 0.006(D_{50(Field,\ mm)})^{-2} \qquad \text{Equation 32}$$

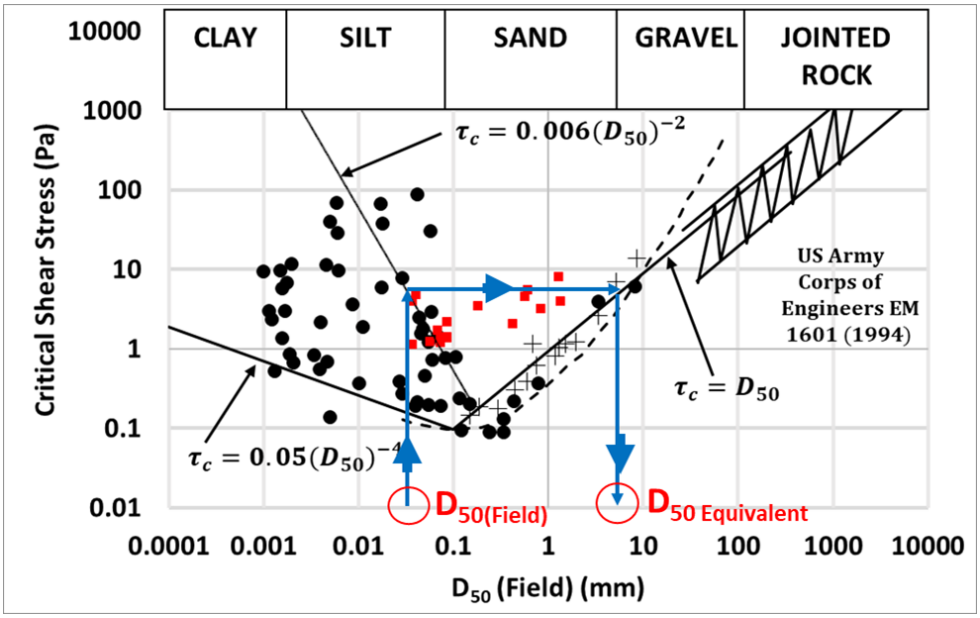

Figure (19): Equivalent Mean Grain Size Derivation Concept

Despite the advantages of the empirical approach presented by Equation 32, the uncertainties are still there, and the excess shear stress parameters are varying significantly between soils. Therefore, the experimental approach may still the best choice if the testing device are available and the conditions are suitable.

4.4 Correlation Between D_{50} and the Erodibility Coefficient

As discussed before, the excess shear stress parameters govern the erosion behavior of the soils. Both critical shear stress and erodibility coefficient are important. As the critical shear stress correlates with the mean grain size diameter, a trial was conducted to apply the same approach on the erodibility coefficient as shown in Figure (20), and Figure (21). However, no clear trend was observed between the erodibility coefficient and the mean grain size neither in arithmetic scale nor in log-log scale.

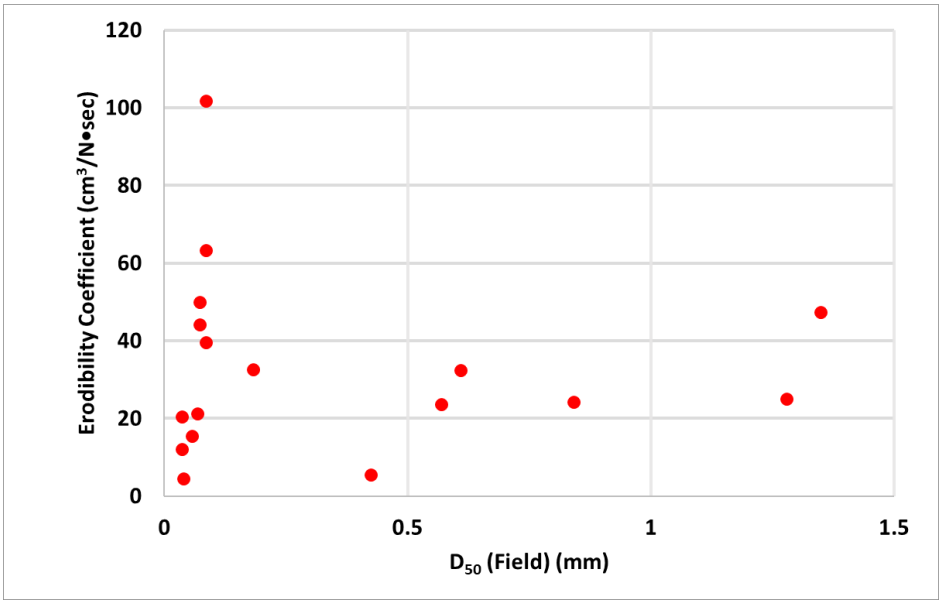

Figure (20): Erodibility Coefficient vs. Mean Grain Size (Arithmetic scale)

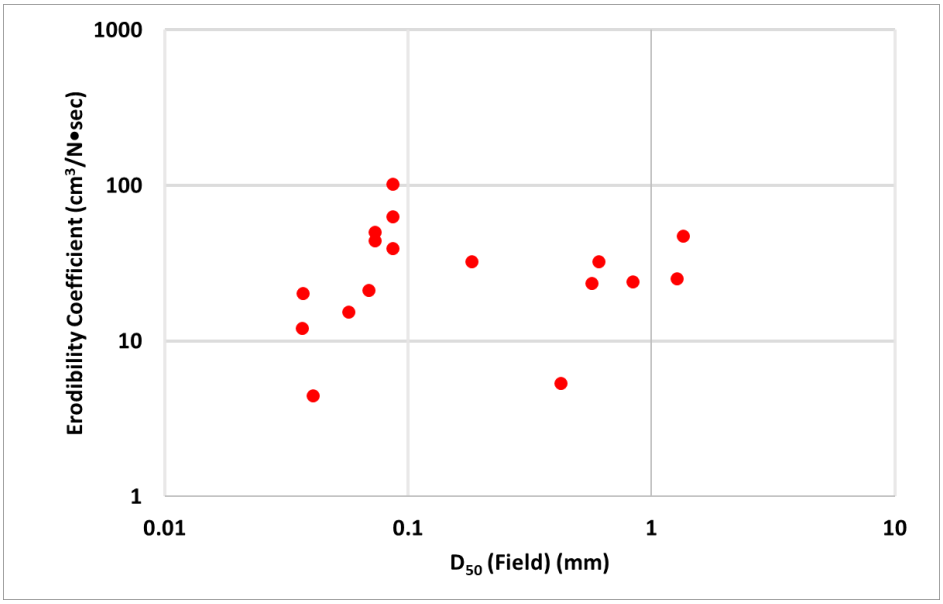

Figure (21): Erodibility Coefficient vs. Mean Grain Size (log-log scale)

Chapter 5

Conclusions, Recommendations, and Future Studies

5.1 Conclusions

This study evaluated the erosion behavior of the riverbed soils in Nebraska around Lincoln. Seventeen riverbed samples were tested in the laboratory using the Mini-JET to obtain the excess shear stress parameters. As a result, the following conclusions were obtained.

- The riverbed erosion test results showed a high erodibility coeffect with a range of 4 – 101 $cm^3/N•sec$.
- The riverbed erosion test results showed critical shear stress within a range of 1 – 8 Pa.
- Based on Briaud et al. (2017) classification, the tested soils classified as a high erodibility geomaterials.
- The test results indicate that the riverbed soils in this area may erode faster (due to the high erodibility coefficient), but to about the same depth (due to the similar critical shear stress) compared with Hanson & Simon (2001) study.
- The test results showed a good match with Briaud et al. (2017) study, indicating that his upper limit equation was applicable for the silty soils in Nebraska around Lincoln.
- The equivalent sand particle diameter for the tested silty soils may be obtained by:

$$D_{50(Sand\ Equivalent,\ mm)} = 0.006(D_{50(Field,\ mm)})^{-2}.$$

- The mean grain size did not show a clear trend when plotted with the erodibility coefficient.

- However, it is recommended to use the experimental approach whenever it is accessible because of the wide range of the excess shear stress parameters, particularly for fine-grained soils.

5.2 Future Studies

- The erosion test results of this study showed a higher erodibility coefficient than several previous studies. One possible reason for this difference may be the existence of expansive menials in the tested riverbed soils in this study. It would be helpful to review the clay mineralogy to validate this possibility.

- This study presented the experimental approach to find the equivalent sand particle diameter to predict the critical shear stress of fine-grained soil. Then, it may be valuable to apply numerical analysis so that the overall effect of the equivalent diameter on the erosion characteristics can be analyzed.

- This Study used the Mini-JET testing device to predict the excess shear stress parameters. The submerged jets, in general, needs to block the flow by turning the nozzle away from the impinging point during the reading, which may lead to different flow conditions. It will be important to understand the effect of this disruption on the erosion results.

- This study used the excess shear stress parameters model, which may have a dimensional trouble when the soil type related empirical parameter is not equal to one. It will be important to work on improving this equation in a way that makes it dimensionally correct.

- The mean grain size (D_{50}) is widely used nowadays to predict the erodibility of the soils. However, it would be beneficial in the future to incorporate other soil properties, such as the overall gradation curve for erosion analysis as well as the traditional soil index parameters such as the plasticity index (PI).

References

Al-Madhhachi, A. T., Hanson, G. J., Fox, G. A., Tyagi, A. K., & Bulut, R. (2011). Measuring Erodibility of Cohesive Soils Using Laboratory Jet Erosion Tests. *World Environmental and Water Resources Congress 2011*.

Al-Madhhachi, A. T., Hanson, G. J., Fox, G. A., Tyagi, A. K., & Bulut, R. (2013). MEASURING SOIL ERODIBILITY USING A LABORATORY "MINI" JET. *Transactions of the ASABE*, *56*(3), 901–910.

Albertson, M. L., Dai, Y. B., Jensen, R. A., & Rouse, H. (1950). Diffusion of Submerged Jets. *Transactions of the American Society of Civil Engineers*, *115*(1).

Blaisdell, F. W., Hebaus, G. G., & Anderson, C. L. (1981). Ultimate Dimensions of Local Scour. *Journal of the Hydraulics Division*, *107*(3).

Briaud, J.-L., Chen, H.-C., Nurtjahyo, P., & Wang, J. (2004). Pier and Contraction Scour in Cohesive Soils. In *Pier and Contraction Scour in Cohesive Soils*. https://doi.org/10.17226/13774

Briaud, J., & Hunt, B. E. (2006). Bridge Scour & the Structural Engineer. *Structure Magazine*, *December*, 58–61.

Briaud, J. L., Ting, F. K., Chen, H. C., Cao, Y., Han, S. W., Kwak, K. W., & Member, S. (2001). *EROSION FUNCTION APPARATUS FOR SCOUR RATE PREDICTIONS*. *5*(February), 105–113.

Briaud, J., Ting, F. C. K., Chen, H. C., Gudavalli, R., Perugu, S., & Member, S. (1999). *SRICOS: PREDICTION OF SCOUR RATE IN COHESIVE SOILS AT BRIDGE PIERS*. *125*(April), 237–246.

Briaud, Jean-Louis. (2015). Scour Depth at Bridges: Method Including Soil Properties. I: Maximum Scour Depth Prediction. *Journal of Geotechnical and Geoenvironmental Engineering*, *141*(2), 04014104. https://doi.org/10.1061/(asce)gt.1943-5606.0001222

Briaud, Jean-Louis, Govindasamy, A. V., & Shafii, I. (2017). Erosion Charts for Selected Geomaterials. *Journal of Geotechnical and Geoenvironmental Engineering*, *143*(10), 04017072. https://doi.org/10.1061/(asce)gt.1943-5606.0001771

Buffington, J. M. (1999). THE LEGEND OF A. F. SHIELDS. *Journal of Hydraulic Engineering*, *125*(4).

Casey, H. J. (1935). "Über Geschiebebewegung." Mitteilungen der Preussischen Versuchsanstalt für Wasserbau und Schiffbau, Springer, Berlin.

Chapuis, R. P., & Gatien, T. (1986). An improved rotating cylinder technique for quantitative measurements of the scour resistance of clays. *Canadian Geotechnical Journal*, *23*(1), 83–87. https://doi.org/10.1139/t86-010

Das, B. M. (2015). *Soil Mechanics Laboratory Manual* (Ninth Edit). Oxford University Press.

Duncan, J. M., & Chang, C.-Y. (1970). Nonlinear Analysis of Stress and Strain in Soils. *Journal of the Soil Mechanics and Foundations Division*, *96*(5).

Gilbert, G. K. (1914). The transportation of debris by running water, USGS, Washington, DC.

Hanson, G. J. (1990). Surface Erodibility of Earthen Channels at High Stresses Part II - Developing an In Situ Testing Device. *Transactions of the American Society of Agricultural Engineers*. https://doi.org/10.13031/2013.31305

Hanson, G. J., & Cook, K. R. (1997). *Development of Excess Shear Stress Parameters for Circular Jet Testing*.

Hanson, G. J., & Cook, K. R. (2004). Apparatus, test procedures, and analytical methods to measure soil erodibility in situ. *Applied Engineering in Agriculture*, *20*(4), 455–462.

Hanson, G. J., & Simon, A. (2001). Erodibility of cohesive streambeds in the loess area of the Midwestern USA. *Hydrological Processes*, *15*(1), 23–38. https://doi.org/10.1002/hyp.149

Hanson, G J. (1990). *Surface Erodibility of Earthen Channels at High Stresses Part I - Open Channel Testing*. *33*.

Hanson, Gregory J., & Hunt, S. L. (2007). Lessons learned using laboratory JET method to measure soil erodibility of compacted soils. *Applied Engineering in Agriculture*, *23*(3), 305–312.

https://education.nationalgeographic.org/resource/erosion (Access Date: June 2022)

Jang, W., Song, C. R., Kim, J., Cheng, A. H.-D., & Al-Ostaz, A. (2011). Erosion Study of New Orleans Levee Materials Subjected to Plunging Water. *Journal of Geotechnical and Geoenvironmental Engineering*, *137*(4), 398–404. https://doi.org/10.1061/(asce)gt.1943-5606.0000439

Kameshwar, S., & Padgett, J. E. (2018). Parameterized Fragility Assessment of Bridges Subjected to Pier Scour and Vehicular Loads. *Journal of Bridge Engineering*, *23*(7), 04018044. https://doi.org/10.1061/(asce)be.1943-5592.0001240

Khanal, A., Fox, G. A., & Al-Madhhachi, A. T. (2016). Variability of Erodibility Parameters from Laboratory Mini Jet Erosion Tests. *Journal of Hydrologic Engineering*, *21*(10), 04016030. https://doi.org/10.1061/(asce)he.1943-5584.0001404

Moore, L., & Masch, F. D. (1962). *Experiments on the Scour Resistance of Cohesive Sediment*. *67*(4).

Nebraska Legislature Transportation and Telecommunications Committee. (2014). The Alarming Conditions of Nebraska's Rural Bridges. L.R. 528 Study Report. Lincoln, Nebraska. https://nebraskalegislature.gov/pdf/reports/committee/transport/2014_lr528.pdf

Partheniades, E. (1965). Erosion and Deposition of Cohesive Soils. *Journal of the Hydraulics Division*, *91*(1).

Rajaratnam, N. (1976). *Turbulent Jets*.

Seed, R. B., Bea, R. G., Abdelmalak, R. I., Athanasopoulos, A. G., Boutwell, G. P., Bray, J. D., Briaud, J.-L., Cheung, C., Cobos-Roa, D., Cohen-Waeber, J., Collins, B. D., Ehrensing, L., Farber, D., & Hanemann, M. (2006). Investigation of the Performance of the New Orleans Flood Protection Systems in Hurricane Katrina on August 29, 2005. *Independent Levee Investigation Team: Final Report*, *I*, 690. http://digitalcommons.calpoly.edu/cgi/viewcontent.cgi?article=1032&context=cenv_fac%0Ahttp://files/2442/New_Orleans_Levee_Breaks.pdf (Chapter 9)

Shields, A. (1936). *Application of similarity principles and turbulence research to bed-load movement*.

Simon, A., Thomas, R. E., & Klimetz, L. (2010). Comparison and Experiences With Field Techniques To Measure Critical. *2nd Joint Federal Interagency Conference, Las Vegas*, *826*, 13.

Song, Chung R., Kim, J., Wang, G., & Cheng, A. H.-D. (2011). Reducing Erosion of Earthen Levees Using Engineered Flood Wall Surface. *Journal of Geotechnical and Geoenvironmental Engineering*, *137*(10), 874–881. https://doi.org/10.1061/(asce)gt.1943-5606.0000500

Song, Chung Rak, Kim, J., Kidd, J. T., Cheng, A., & Admiraal, D. (2018). Effect of thickness of planar nozzles on erosion depth of levee soils subjected to plunging water. *International Journal of Sediment Research*, *33*(3), 243–249. https://doi.org/10.1016/j.ijsrc.2018.04.010

Stein, O. R., Julien, P. Y., & Alonso, C. V. (1993). Mechanics of jet scour downstream of a headcut. *Journal of Hydraulic Research*, *31*(6).

T. Kidd, J., R. Song, C., Al-Ostaz, A., H. -D. Cheng, A., & Jang, W. (2011). Erosion Control Using Modified Soils. *International Journal of Erosion Control Engineering*, *4*(1), 1–9. https://doi.org/10.13101/ijece.4.1

USACE (U.S. Army Corps of Engineers). (1936). "Flume tests made to develop a synthetic sand which will not form ripples when used in movablebed models." Technical Memorandum 99-1, Vicksburg, MS.

Vanoni, V. (1975). Sedimentation engineering, ASCE, New York.

White, C. M. (1940). The equilibrium of grains on the bed of a stream. *Proceedings of the Royal Society of London. Series A. Mathematical and Physical Sciences*, *174*(958), 322–338. https://doi.org/10.1098/rspa.1940.0023

Appendix A

Gradation Curves

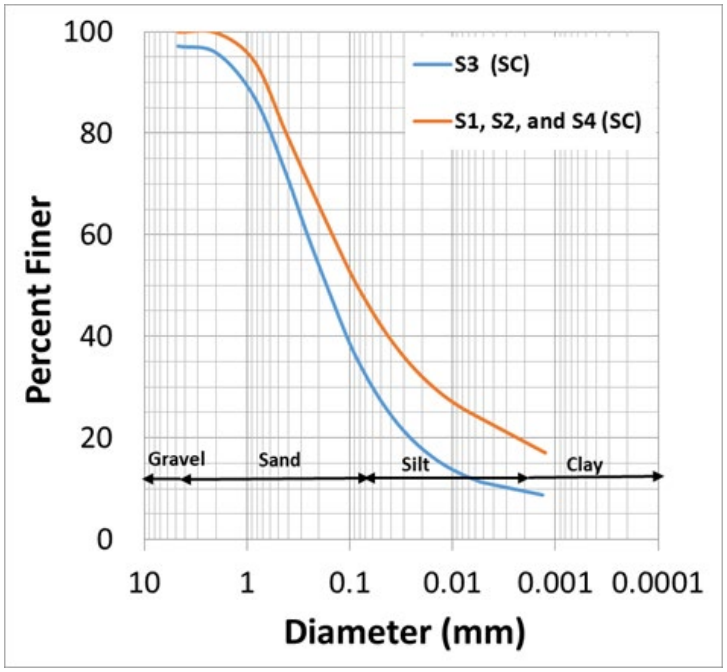

Figure (22): Gradation Curves for Lincoln Site Soils

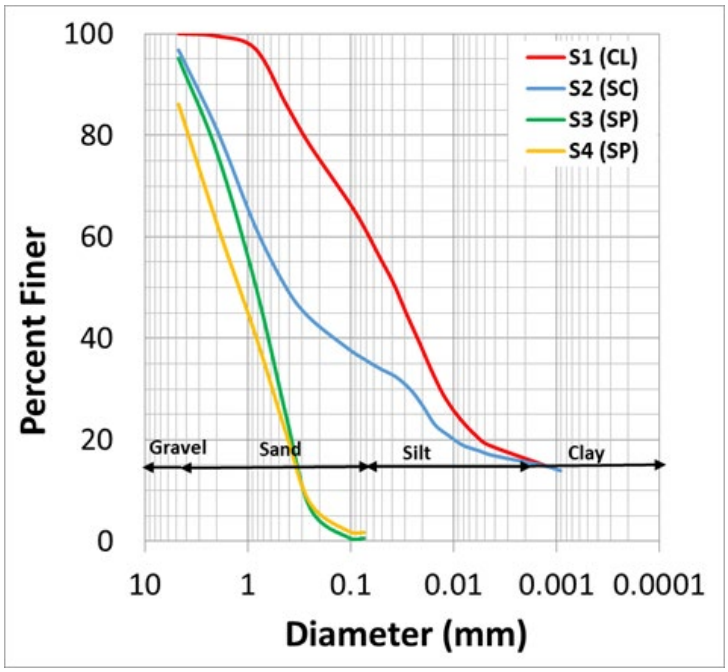

Figure (23): Gradation Curves for Wilber Site Soils

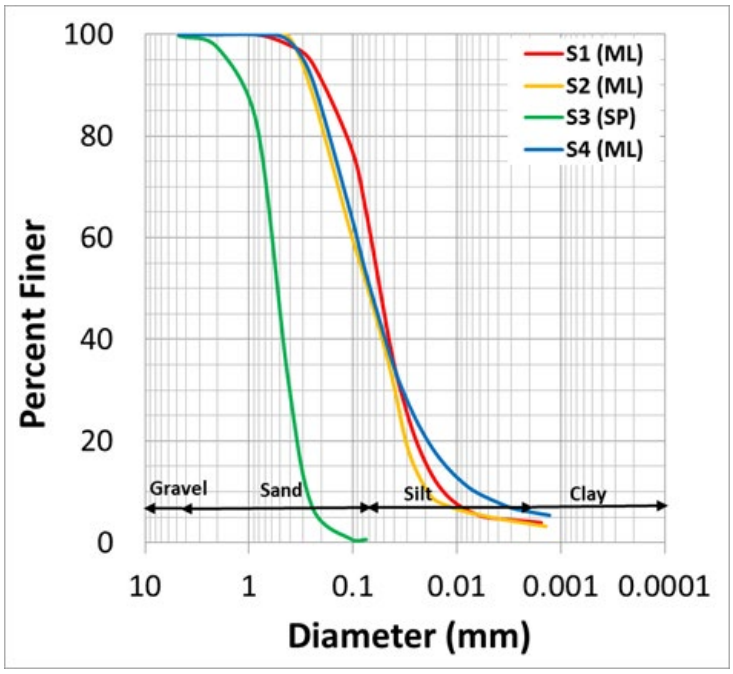

Figure (24): Gradation Curves for Hooper Site Soils

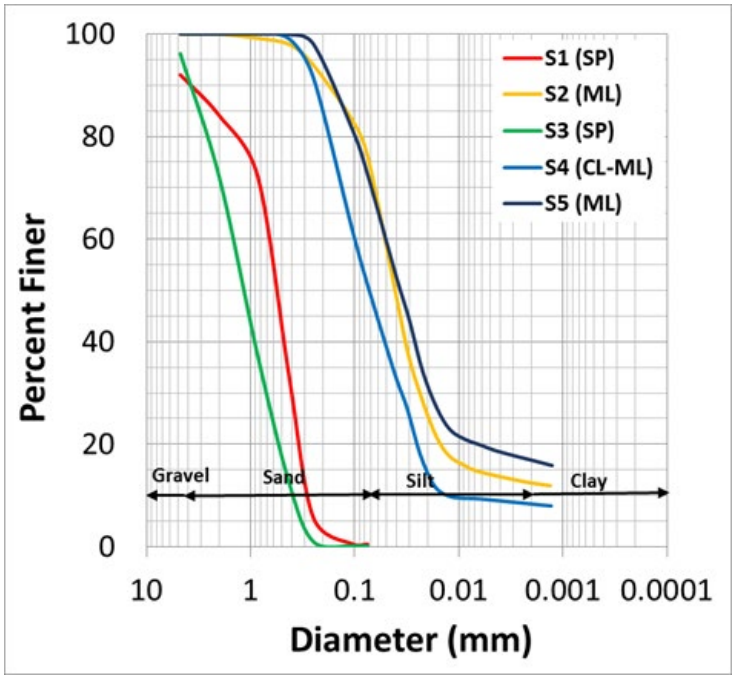

Figure (25): Gradation Curves for Beatrice Site Soils

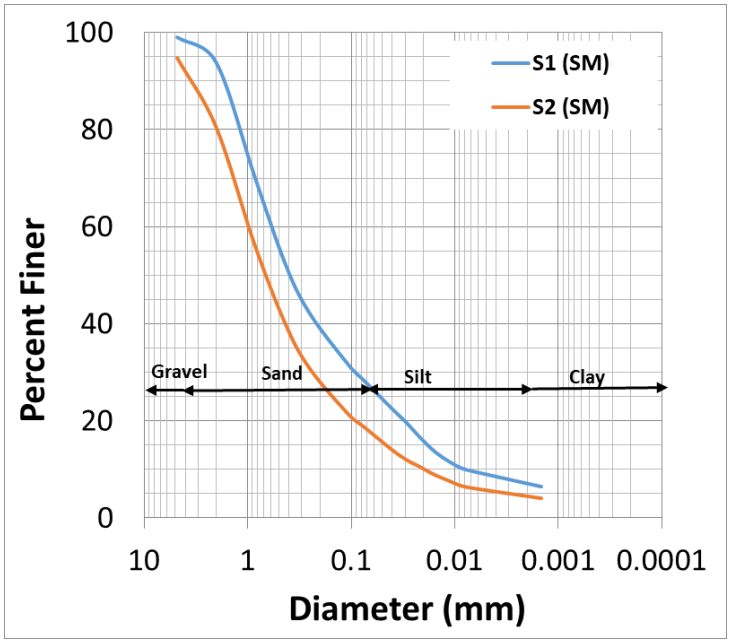

Figure (26): Gradation Curves for UNL City Campus Soils

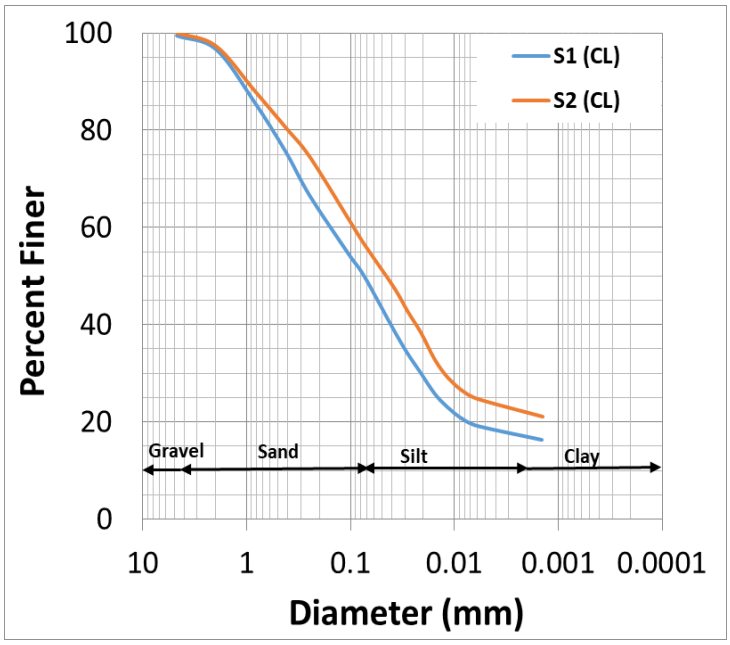

Figure (27): Gradation Curves for UNL East Campus Soils

Appendix B

Mini-JET Data with Back Calculation

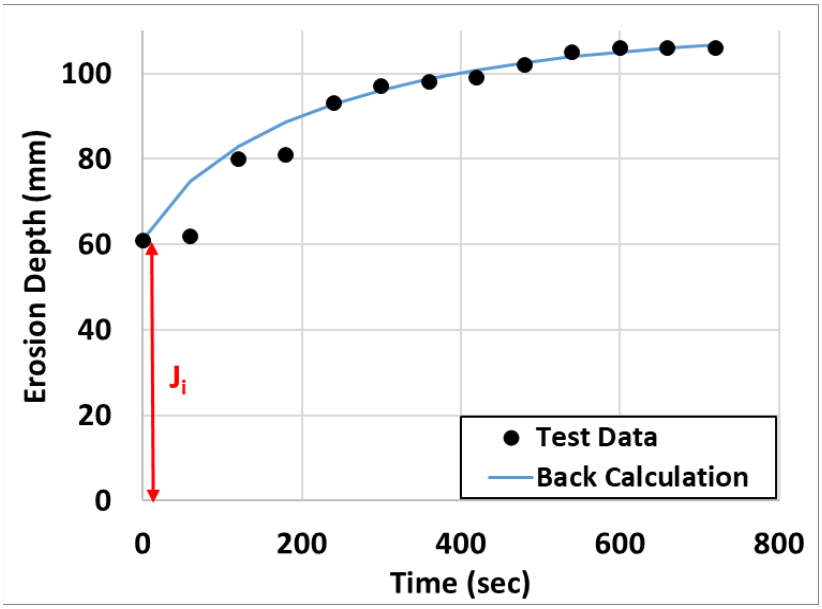

Figure (28): Depth Gauge Reading vs. Time for Lincoln Site Sample 1 (Note: J_i is the initial distance from the nozzle to the soil surface)

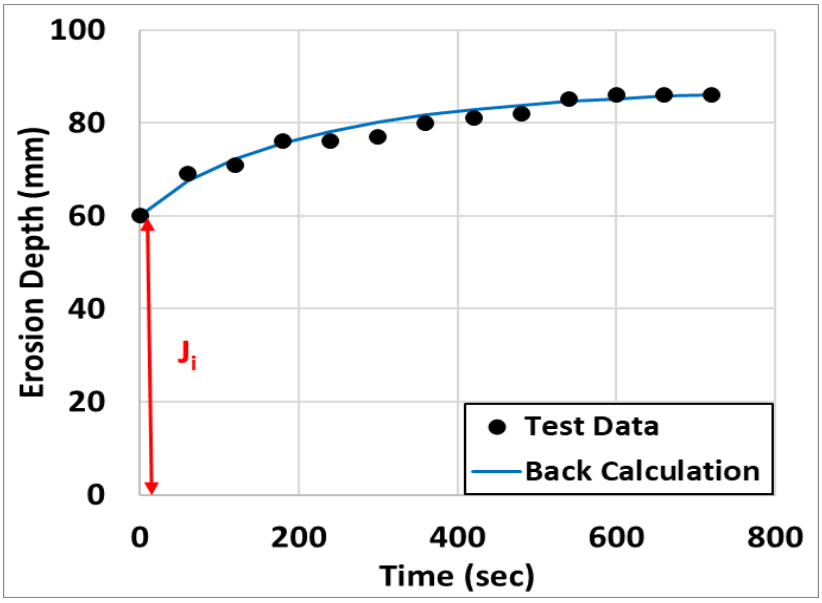

Figure (29): Depth Gauge Reading vs. Time for Lincoln Site Sample 2 (Note: J_i is the initial distance from the nozzle to the soil surface)

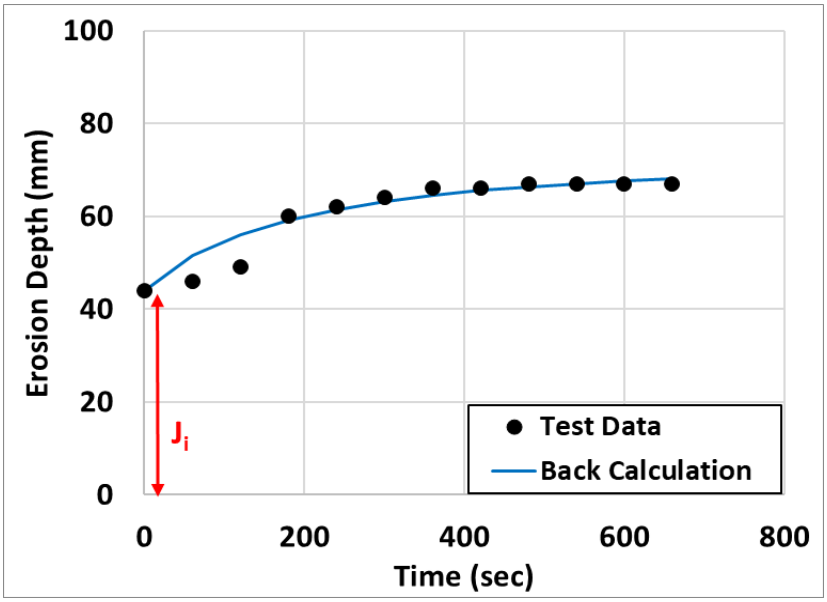

Figure (30): Depth Gauge Reading vs. Time for Lincoln Site Sample 3 (Note: J_i is the initial distance from the nozzle to the soil surface)

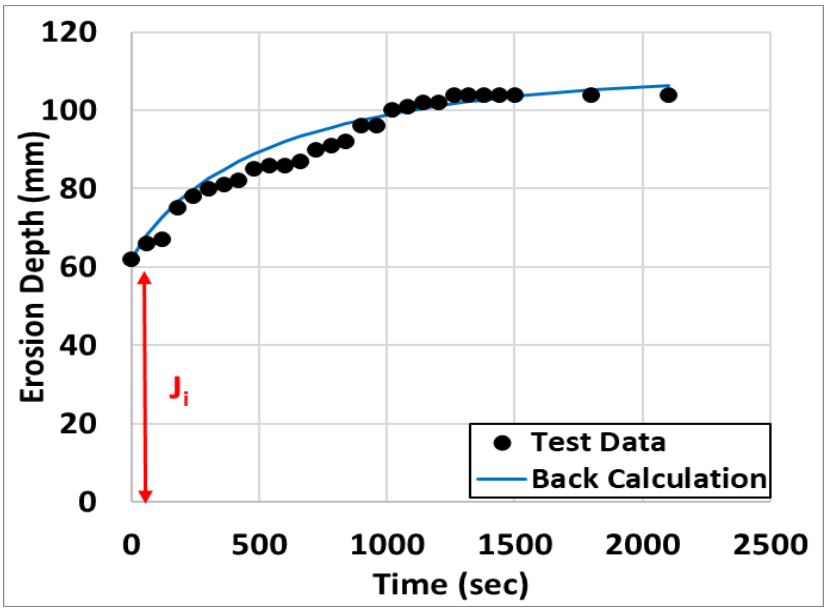

Figure (31): Depth Gauge Reading vs. Time for Lincoln Site Sample 4 (Note: J_i is the initial distance from the nozzle to the soil surface)

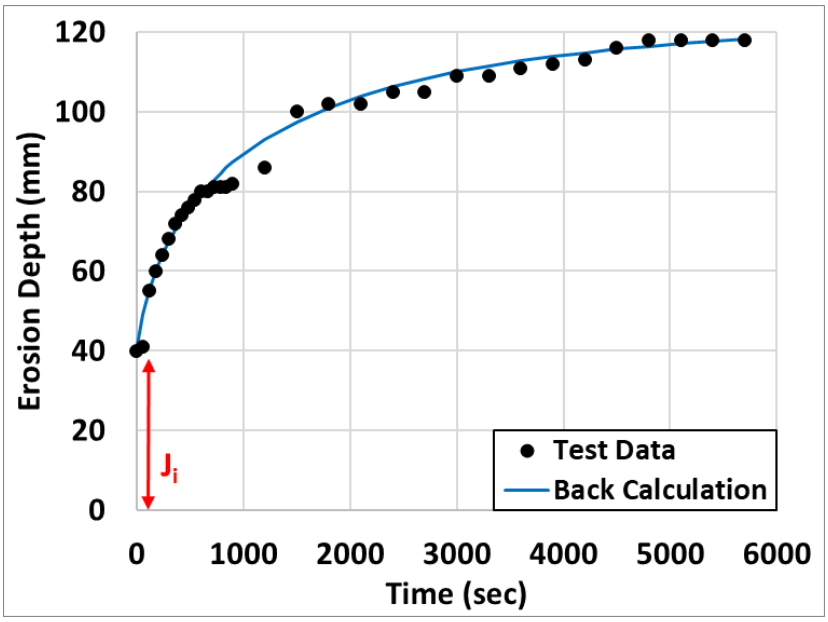

Figure (32): Depth Gauge Reading vs. Time for Wilber Site Sample 1 (Note: J_i is the initial distance from the nozzle to the soil surface)

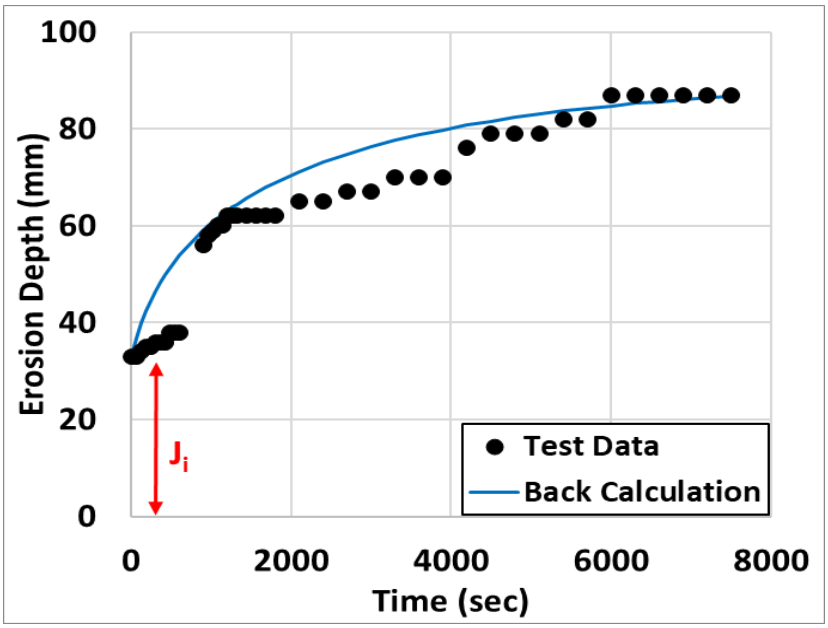

Figure (33): Depth Gauge Reading vs. Time for Wilber Site Sample 2 (Note: J_i is the initial distance from the nozzle to the soil surface)

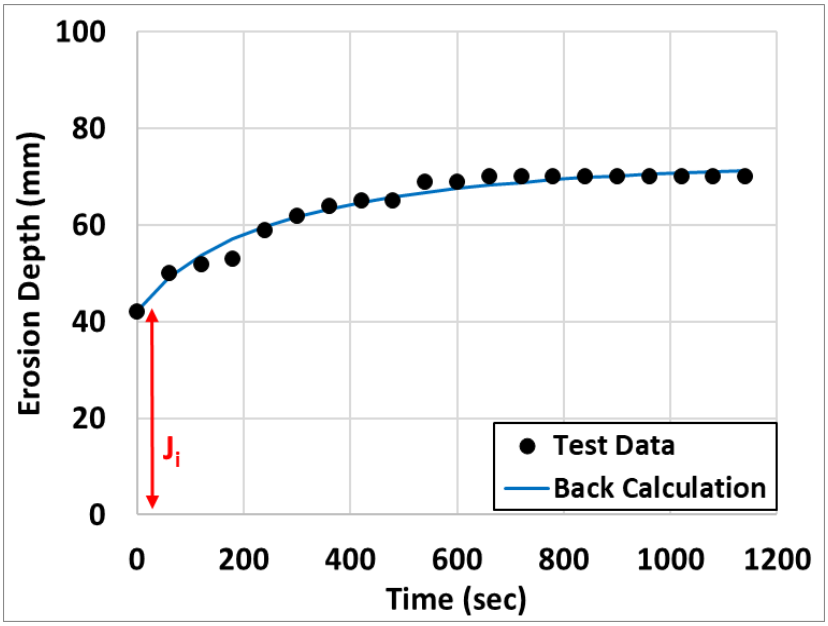

Figure (34): Depth Gauge Reading vs. Time for Wilber Site Sample 3 (Note: J_i is the initial distance from the nozzle to the soil surface)

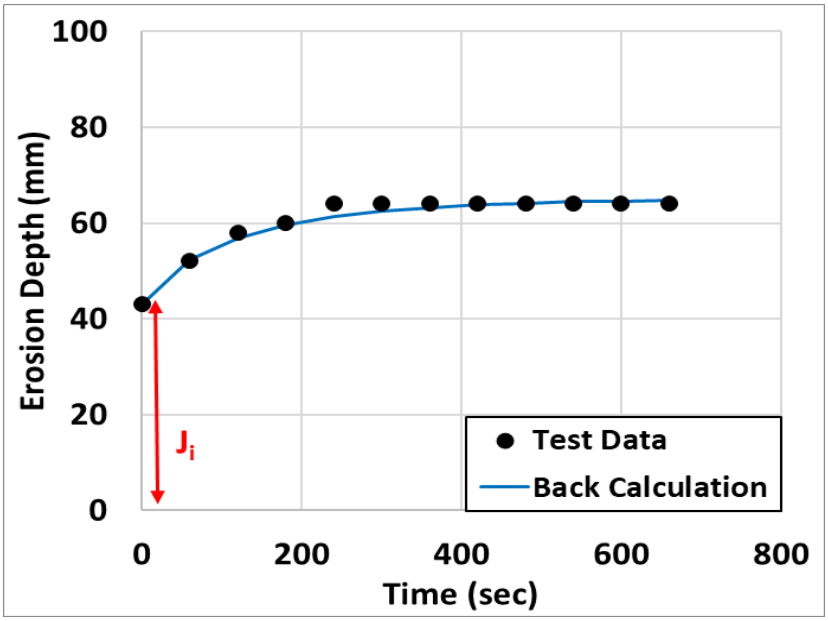

Figure (35): Depth Gauge Reading vs. Time for Wilber Site Sample 4 (Note: J_i is the initial distance from the nozzle to the soil surface)

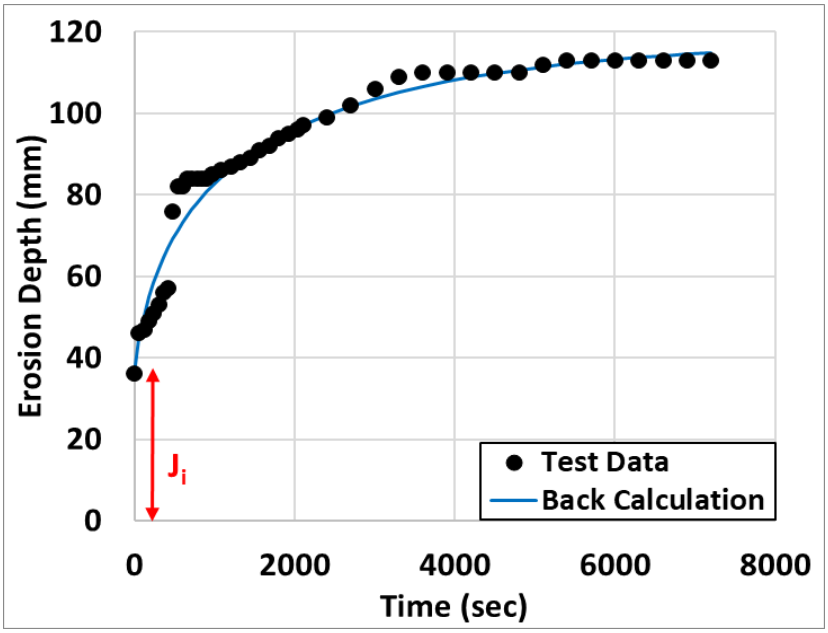

Figure (36): Depth Gauge Reading vs. Time for Hooper Site Sample 1 (Note: J_i is the initial distance from the nozzle to the soil surface)

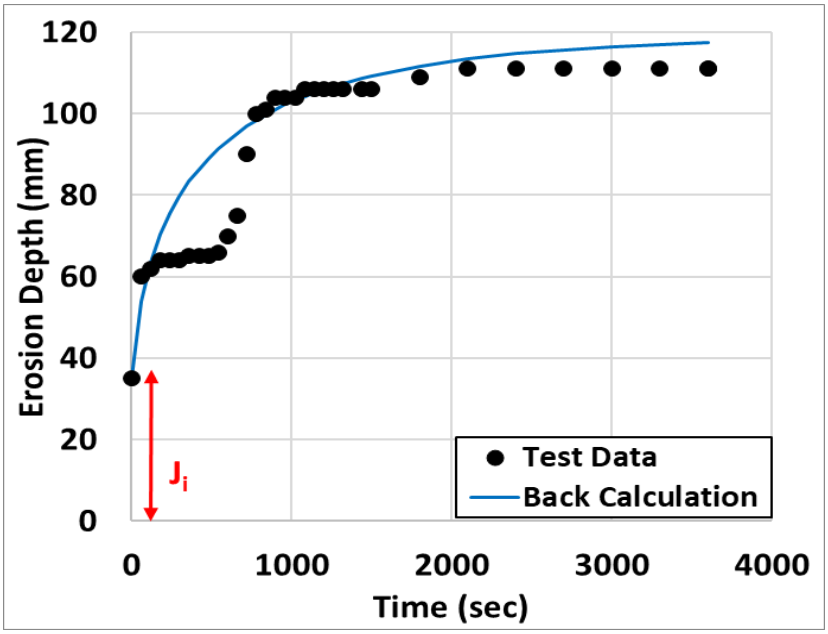

Figure (37): Depth Gauge Reading vs. Time for Hooper Site Sample 2 (Note: J_i is the initial distance from the nozzle to the soil surface)

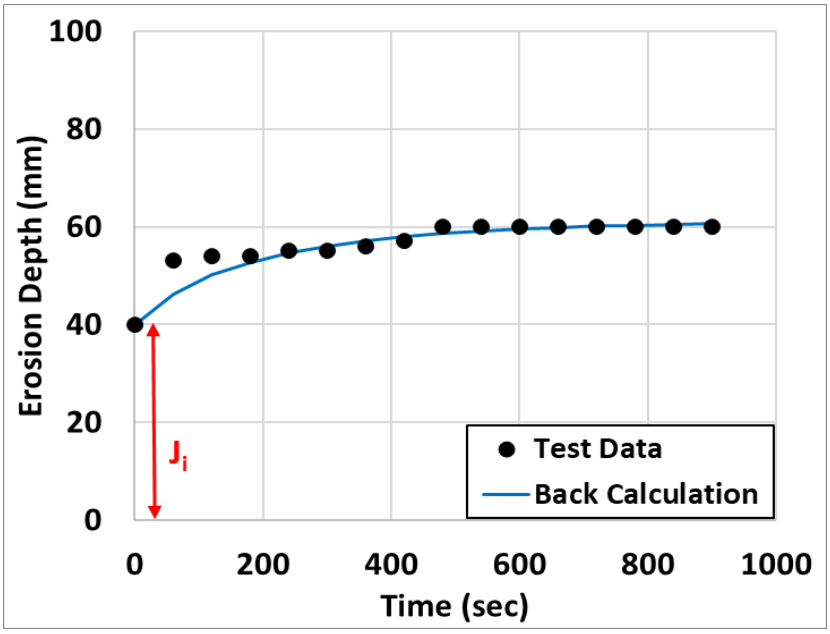

Figure (38): Depth Gauge Reading vs. Time for Hooper Site Sample 3 (Note: J_i is the initial distance from the nozzle to the soil surface)

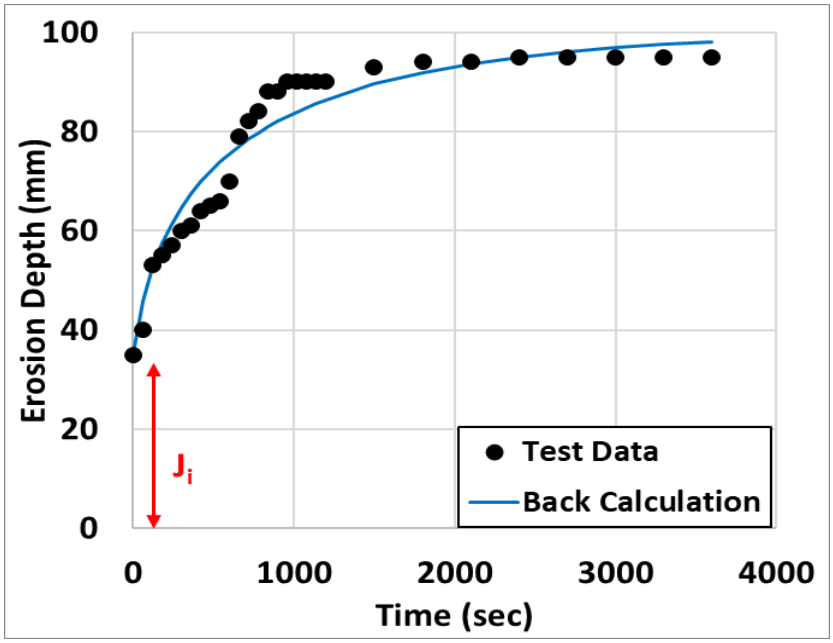

Figure (39): Depth Gauge Reading vs. Time for Hooper Site Sample 4 (Note: J_i is the initial distance from the nozzle to the soil surface)

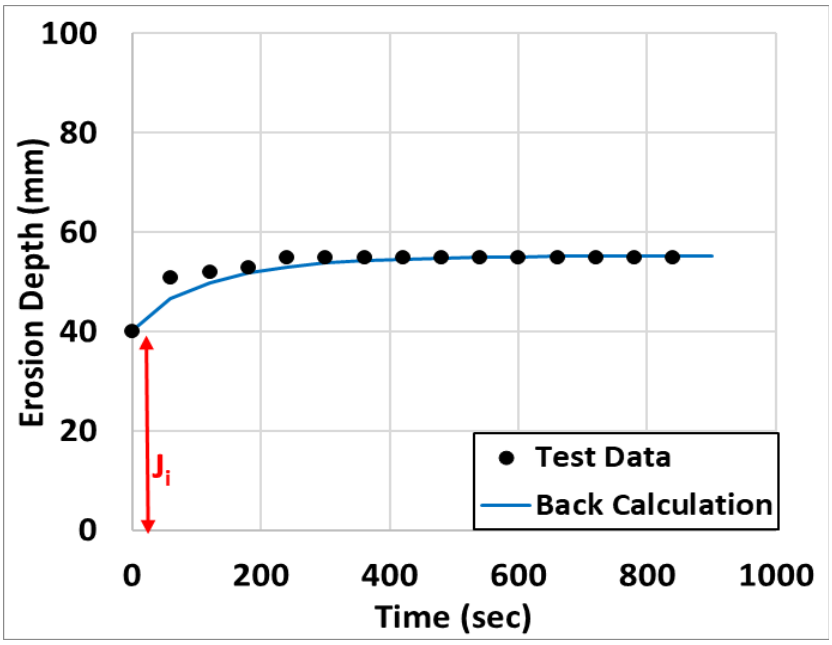

Figure (40): Depth Gauge Reading vs. Time for Beatrice Site Sample 1 (Note: J_i is the initial distance from the nozzle to the soil surface)

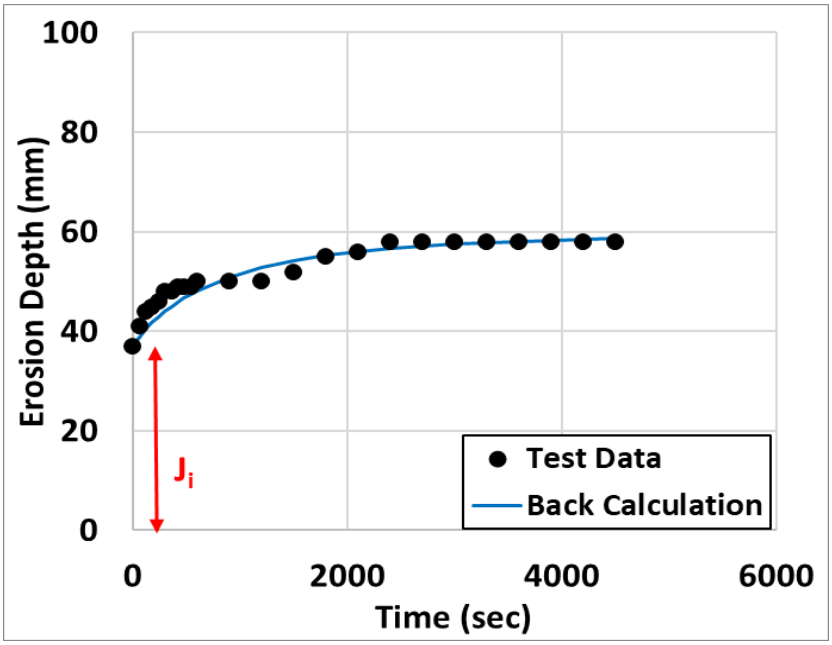

Figure (41): Depth Gauge Reading vs. Time for Beatrice Site Sample 2 (Note: J_i is the initial distance from the nozzle to the soil surface)

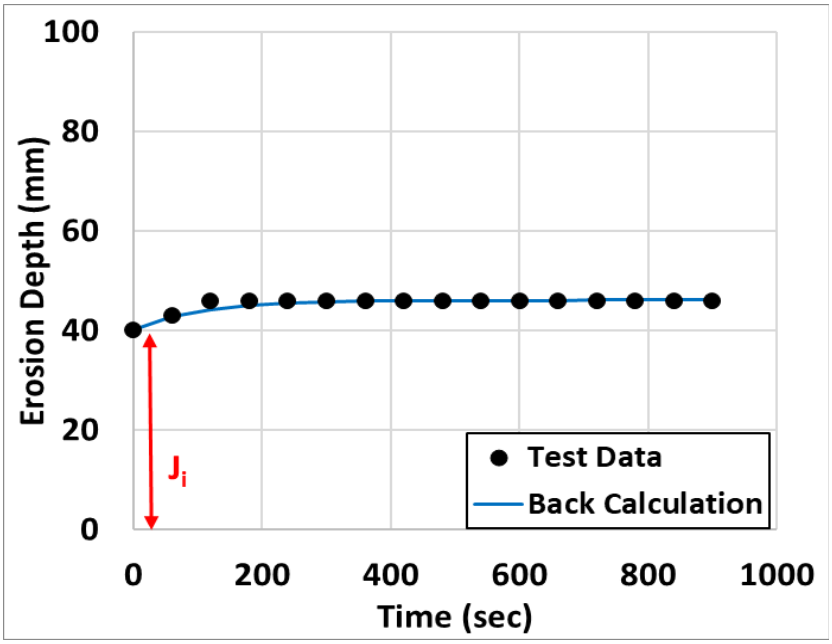

Figure (42): Depth Gauge Reading vs. Time for Beatrice Site Sample 3 (Note: J_i is the initial distance from the nozzle to the soil surface)

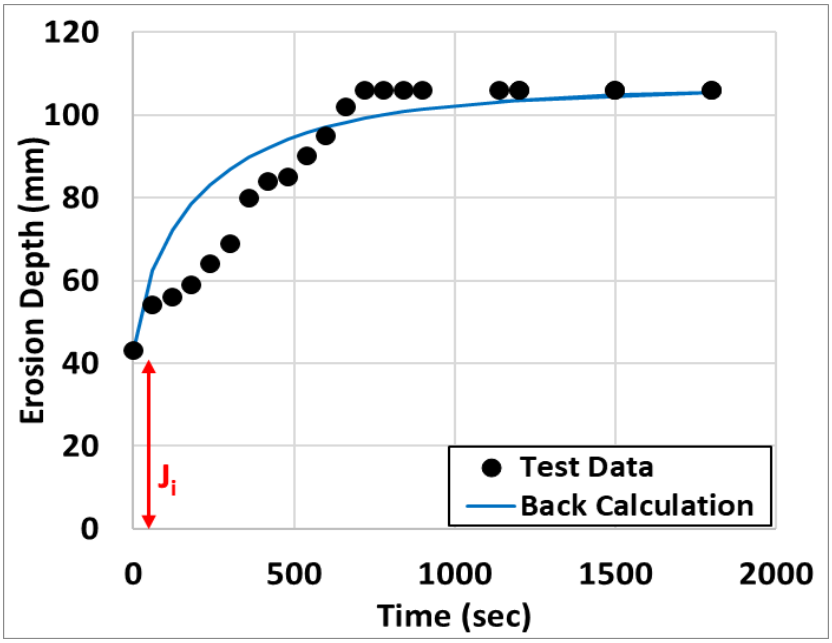

Figure (43): Depth Gauge Reading vs. Time for Beatrice Site Sample 4 (Note: J_i is the initial distance from the nozzle to the soil surface)

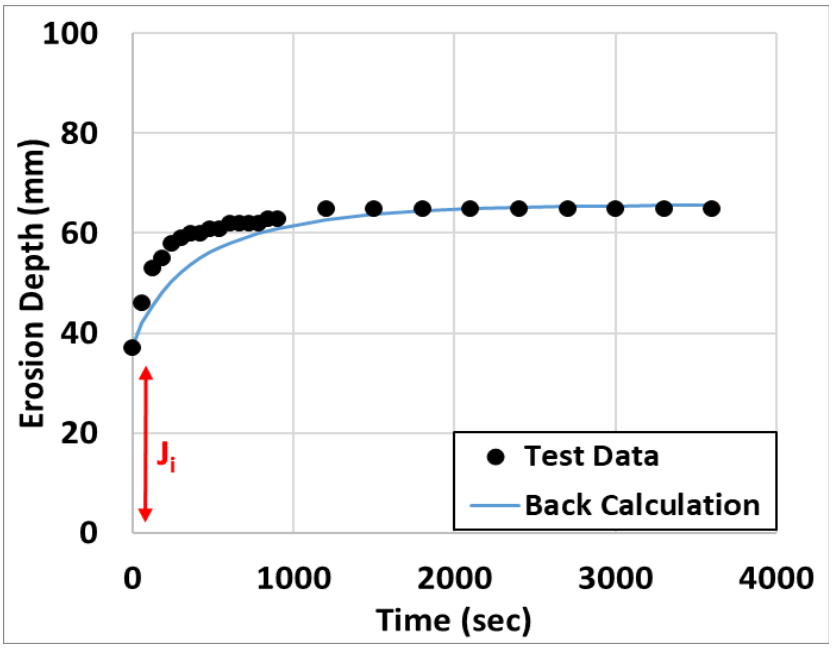

Figure (44): Depth Gauge Reading vs. Time for Beatrice Site Sample 5 (Note: J_i is the initial distance from the nozzle to the soil surface)

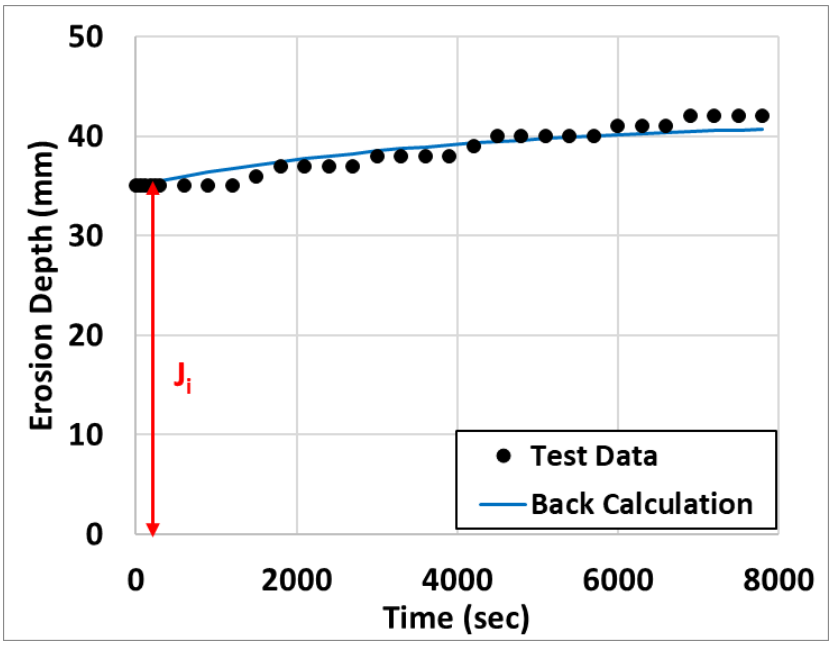

Figure (45): Depth Gauge Reading vs. Time for UNL City Campus Sample 1 (Note: J_i is the initial distance from the nozzle to the soil surface)

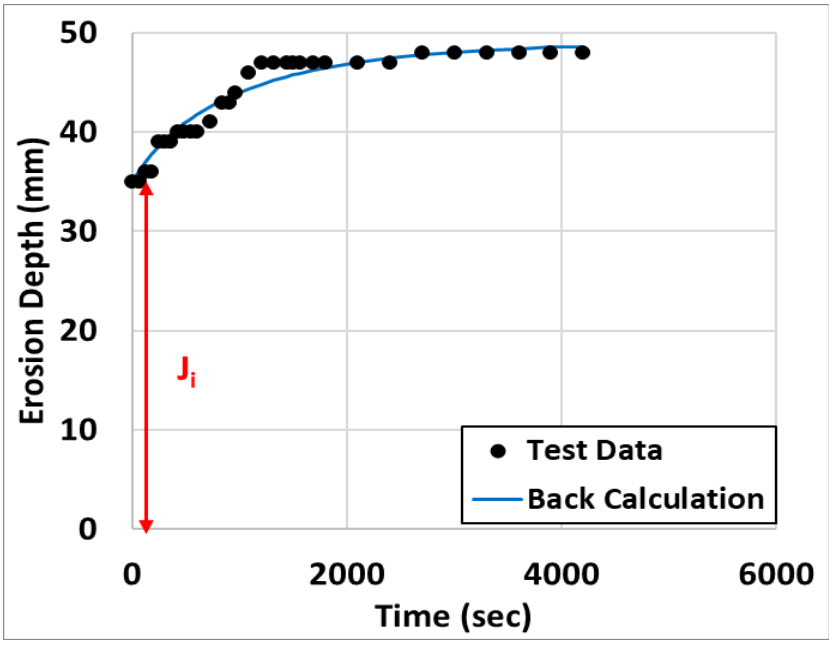

Figure (46): Depth Gauge Reading vs. Time for UNL City Campus Sample 2 (Note: J_i is the initial distance from the nozzle to the soil surface)

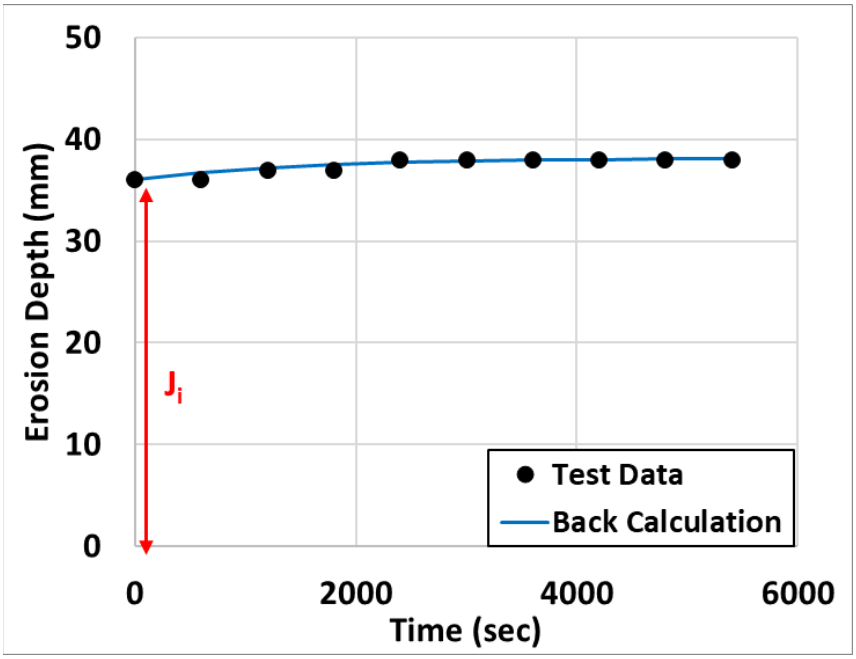

Figure (47): Depth Gauge Reading vs. Time for UNL East Campus Sample 1(Note: J_i is the initial distance from the nozzle to the soil surface)

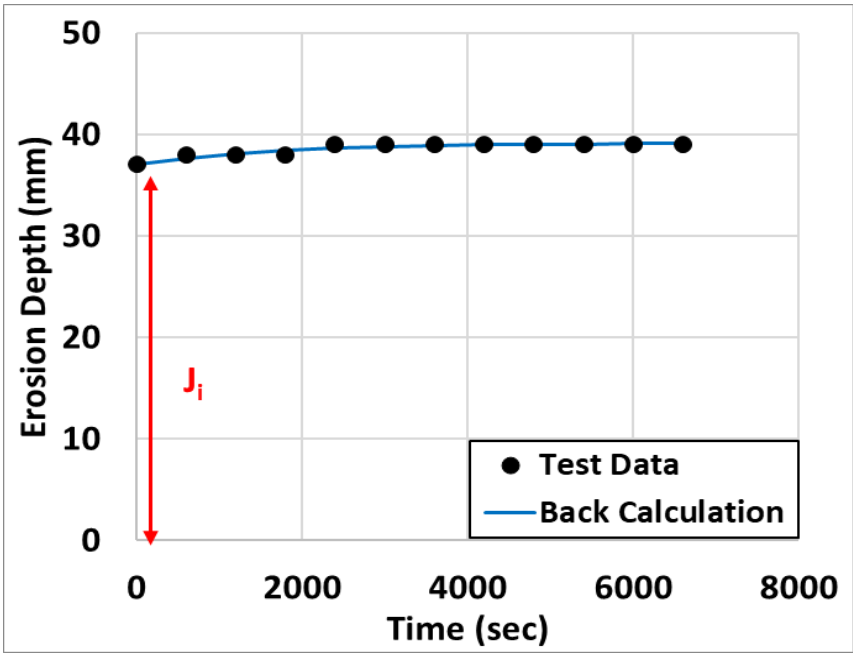

Figure (48): Depth Gauge Reading vs. Time for UNL City Campus Sample 2 (Note: J_i is the initial distance from the nozzle to the soil surface)